UNIVERSITY OF TARTU
Faculty of Science and Technology
Institute of Physics

Ahmet Burak Baloglu

Materials Science and Technology
Master's Thesis (30 ECTS)

Graphene in blister-based LIFT

Supervisors: Prof. Raivo Jaaniso
Dr Margus Kodu

Laboratory of Sensor Technologies
Institute of Physics
University of Tartu

Tartu 2023

Graphene in blister-based LIFT

Abstract

Laser-induced forward transfer (LIFT) can provide a clean (non-contact and solvent-free) technique for the high-resolution printing of two-dimensional materials, a significant technological step for their integration into microdevices. The blister-based (BB) version of LIFT allows the transfer of ultra-thin layers without damaging the materials on the receiving substrate with intense laser light. This work investigated single-layer graphene in different roles as a donor, acceptor and release material in BB-LIFT. The transfer of graphene and ultrathin oxide (ZrO_2) layers was confirmed and characterised through optical microscopy, Raman spectroscopy and scanning electron microscopy (SEM). The crucial role of the graphene interlayer in ZrO_2 transfer was revealed. The immediate motivation for the work was the improvement of graphene-based gas sensors by transferring ultrathin oxides as gas sensor receptor layers on the CVD graphene as a transducer layer. It was found that the sensitivity of sensors to trace level NO_2 gas did not practically increase after BB-LIFT of ultrathin (0.5-50 nm) ZrO_2 layers. This was interpreted as a lack of strong interactions of the transferred oxide flakes (and a small contact area) with the graphene layer of the sensor substrate. In order to increase the interaction, the sensors were annealed at a higher temperature (up to 500 °C in a vacuum), which significantly accelerated the gas response. The work highlights the finding that the oxide layer can be transferred only when graphene is inserted between the blister and oxide layers. This is a novel application for graphene, considerably widening the scope of materials transferable by BB-LIFT.

Keywords: blister-based laser-induced forward transfer (BB-LIFT); graphene; ZrO_2; NO_2 sensor

CERCS: P260 Condensed matter: electronic structure, electrical, magnetic and optical properties, superconductors, magnetic resonance, relaxation, spectroscopy; T165 Laser technology; T155 Coatings and surface treatment.

Grafeen mullipõhises laser-indutseeritud edasikandes

Lühikokkuvõte

Laser-indutseeritud ülekanne (ingl *laser-induced forward transfer* e LIFT) võib pakkuda puhast (kontakti- ja lahustivaba) ja kõrge eraldusvõimega kahemõõtmeliste materjalide trükitehnikat, mis on oluline nende integreerimiseks mikroseadmetesse. LIFTi mullipõhine (ingl *blister-based* e BB) versioon võimaldab üliõhukesi kihte üle kanda ilma vastuvõtval alusel olevaid materjale intensiivse laservalgusega kahjustamata. Selles töös uuriti ühekihilist grafeeni erinevates rollides: doonori, aktseptori ja nn vabastava materjalina BB-LIFT protsessis. Grafeeni ja oksiidi (ZrO_2) üliõhukeste kihtide ülekandmine kinnitati ja karakteriseeriti optilise mikroskoopia, Raman spektroskoopia ja skaneeriva elektronmikroskoopia (SEM) abil. Seejuures selgus grafeeni vahekihi otsustav roll ZrO_2 ülekandes. Töö vahetuks motivatsiooniks oli grafeenipõhiste gaasisensorite täiustamine, kandes üliõhukesed oksiidid sensori retseptorkihtideks CVD grafeenile kui muundurkihile. Selgus, et sensorite tundlikkus väikese koguse NO_2 gaasi suhtes praktiliselt ei suurenenud pärast üliõhukeste (0,5-50 nm) ZrO_2 kihtide BB-LIFT-i. Seda tõlgendati kui ülekantud oksiidihelveste tugeva interaktsiooni puudumist (ja nende väikest kontaktpinda) sensoraluse grafeenikihiga. Interaktsiooni suurendamiseks lõõmutati andureid kõrgemal temperatuuril (vaakumis kuni 500 ^oC), mis kiirendas oluliselt sensori reaktsiooniaega. Töö väljapaistvaks tulemuseks on, et oksiidikihti saab üle kanda ainult siis, kui mulli moodustava materjali ja oksiidikihi vahele on paigutatud grafeen. See on uudne grafeeni rakendus, mis laiendab märkimisväärselt BB-LIFT tehnika poolt ülekantavate materjalide hulka.

Võtmesõnad: mullipõhine laser-indutseeritud edasikanne (BB-LIFT); grafeen; ZrO_2; NO_2 sensor

CERCS: P260 Tahke aine: elektrooniline struktuur, elektrilised, magneetilised ja optilised omadused, ülijuhtivus, magnetresonants, spektroskoopia; T165 Lasertehnoloogia; T155 Pinded ja pinnatehnoloogia.

Table of Contents

Abbreviations

GBGS	Graphene-based gas sensor
LIFT	Laser-induced forward transfer
BB-LIFT	Blister-based laser-induced forward transfer
SEM	Scanning electron microscope
UV	Ultraviolet
CVD	Chemical vapour deposition

1. Introduction

Blister-based laser-induced forward transfer (BB-LIFT) is a variation of the laser-induced forward transfer (LIFT) method designed specifically for the rapid transfer of thin materials at room temperature without requiring vacuum conditions or post-chemical treatment. Unlike other LIFT methods, BB-LIFT utilises a thin metal layer to induce a blister effect, facilitating material transfer onto a substrate. Additionally, this metal layer serves as a protective barrier for the transferred material. In contrast, the conventional LIFT method does not employ an additional sacrificial layer; instead, it solely consists of the material intended for transfer.

Previous applications of LIFT techniques have demonstrated promising results in transferring various materials in different dimensional forms (0D, 1D, 2D, and 3D). While further investigation is needed to understand the influence of 2D materials, such as graphene, on the transfer mechanism, these printing methods have found applications in diverse sectors, including transistors, printed electronic circuits, and particularly in sensor applications.

According to the recent World Health Organization (WHO) Global Air Quality Guidelines [1], air pollution is recognised as the most significant environmental risk to human health. It increases the risk of cardiovascular, respiratory diseases, and lung cancer mortality and potentially affects other organs. By WHO, the yearly recommended air quality levels of the major air pollutant such as nitrogen dioxide (NO_2) is determined as ~5 parts-per-billion (ppb) (conversion factors: at 20 ℃ and 1013 hPa). Thus, producing highly sensitive gas sensors for continually detecting air pollutants at the ppb level is vitally important.

Although previous studies have explored the utility of various types of gas sensors for detecting toxic gases, several challenges persist in their sensing characteristics, including sensitivity, selectivity, response and recovery time, working temperature, and limit of detection as well as challenges related to compactness and high cost. As a result, current gas sensors necessitate further development to enhance these critical parameters.

In particular, the functionalisation of graphene-based gas sensors has been reported to yield exceptional sensing characteristics towards a wide range of gases. Numerous methods, such as pulsed laser deposition (PLD) and chemical vapour deposition (CVD), have been employed to introduce materials onto the surfaces of gas sensors [4]. Nevertheless, it is essential to acknowledge that these techniques have drawbacks, including slow processing, potential residue formation resulting from chemical treatments, and elevated costs.

In this study, the role of graphene as a donor substrate, receiver substrate, and release layer in the blister-based LIFT was investigated. Furthermore, the potential applications of the BB-LIFT method for the functionalisation of graphene gas sensors with graphene and metal oxide (ZrO_2) were explored. The BB-LIFT experiments utilising the KrF excimer laser, electrical gas sensing measurements of the graphene sensors, and sample preparations have been conducted in the Sensor Technology Laboratories at the University of Tartu. Additionally, characterisation techniques such as optical microscopy, Raman spectroscopy and SEM have been employed to characterise the samples in the Institute of Physics Laboratories at the University of Tartu. To maintain simplicity and clarity in this thesis, the term "LIFT" will be used to refer to the BB-LIFT process.

The main objectives of this study are as follows:

- To explore the role of graphene as both a donor and receiver substrate, as well as a release layer for transfer in the BB-LIFT process.
- To investigate the potential of the BB-LIFT technique for the functionalisation of the graphene sensors via metal oxides (ZrO_2) for NO_2 gas sensing.

2. Literature Review

2.1 Graphene as a Material for Gas Sensing

Since the AK. Geim and KS. Novoselov produced the first single-layer graphene using the mechanical exfoliation method and proved its superior electrical properties, bringing them the Nobel Prize in physics in 2010 [2]; graphene became the great focus of interest for possible sensor applications. The very first published gas sensing experiment of a GBGS did by F. Schedin et al. in 2007 [3]. This work demonstrated the step-like changes in resistance related to altered local carrier concentration by a single electron when gas molecules adsorbed on the graphene surface. Moreover, the Hall measurement showed that while oxidising molecules such as NO_2 and oxidane (H_2O) acted as electron acceptors, ammonia (NH_3) and carbon monoxide (CO) served as donors, allowing graphene to behave as an electron and hole carrier. Since then, GBGSs have become a blazing star among researchers who seek to achieve highly sensitive gas sensors. F. Schedin et al. also emphasised the high signal-to-ratio level of the graphene by indicating its high surface area for adsorbents, high conductivity, minimal crystal defects and low resistance. Also, due to its atomic thickness, graphene enables direct interaction between all of its carbon atoms and the analyte, which holds the potential for superior sensitivity. Such significant structural and electrical properties of graphene make it ideal for high-sensitivity gas sensing applications.

The sensing mechanism of GBGSs hinges on the alteration in electrical responses concerning the existence of gaseous molecules. Upon detecting gases within the environment, the carrier concentration in the graphene changes and the sensor generates a conductance difference in proportion to the gas concentration, which can be measured in terms of current or resistance values [4].

The gas sensing of the GBGS starts on the surface. Gaseous molecules are adsorbed on graphene, which causes electron transfer; thus, a change in current is observed. Adsorption on the surface is followed by desorption once the gas flushing stops. This is a reversible process, as the graphene structure will remain unaffected. The sensing mechanism of the GBGSs is determined by the type of doping of the graphene due to the production method. When an oxidising gas such as NO_2 is introduced on the p-type doped graphene, electrons will transfer from the graphene, as NO_2 is a strong electron receiver. Thus, the current will increase as the main carriers of the graphene are holes. In the case of n-type doped graphene, under the NO_2 gas, the sensor's current will decrease as, this time, the main carriers are electrons. The graphene production with the CVD method might

leave some residues of the polymethyl methacrylate (PMMA), photoresist and/or water, which causes p-type doping [5,6].

2.2 Improvements in Graphene-based Gas Sensors

The sensing properties of GBGSs produced by different production methods have previously been demonstrated to detect various gases [7-9]. Even though the gas-sensing properties of GBGSs are powerful, PG has limited sensitivity due to its relatively weak adsorption capacity and nonpolar and inert nature. However, improvements in sensitivity, response, recovery, selectivity and stability could be achieved by different physical and chemical treatments. Thus, essential features could be improved to enhance cost-effectiveness and adaptability for manufacturing. Numerous physical and chemical modification methods have been previously utilised to enhance sensing characteristics. Despite the possibility of expanding the number of techniques through integrating existing practices or implementing innovative methods, this review will solely focus on commonly used methods to achieve a clear and concise classification.

Functionalisation is modifying the surface with specific materials or molecules to gain a better sensitivity in addition to selectivity. Nanoparticles, metal oxides, organic molecules and polymers are common materials for functionalisation applications. Recent reports indicate that the functionalisation of CVD graphene with co-porphyrin resulted in a six-fold increase in sensitivity compared to the non-functionalised GBGS when exposed to 2 ppm NH_3 gas concentration. This is attributed to the larger number of adsorption sites available on the functionalised GBGS. The resulting sensor structure has not only enhanced sensitivity but also selectivity to hydrogen (H_2) gas in rapid humidity changes, which is particularly important for distinguishing different gases in medical breath checkup applications [10].

Doping is another method that introduces impurities and defects to the sensing material, such as graphene. These impurities can be achieved by doping foreign atoms or molecules, which alter the electronic properties of the sensor and can improve its sensing capabilities. According to a recent study, the sensitivity of the pristine GBGS to NH_3 can be enhanced by a factor of seven when exposed to 80 ppm of NH_3 gas in the air after NO_2 doping of the sensor for a period of 50 minutes under 100 ppm of NO_2 gas at 500 Torr and room temperature. Additionally, the doped sensor has shown an improvement in the estimated detection limit, which is approximately 200 ppb, compared to the PG sensor, whose estimated detection limit is about 1.4 ppm. When graphene is

doped with atoms, it causes small changes in the structure and electronic states of the material near the dopant atoms, which makes it easier for gas molecules to attach. Even though NO_2 molecules do not cause any damage to the structure of graphene, they change the electronic states near the Dirac point, making graphene more hole-doped and electron-deficient, which increases the ability of graphene to bind and transfer charges with NH_3 molecules [11]. Another study revealed that the boron-doped GBGS could increase the sensitivity to NO_2 and NH_3 by 27 and 105 times, respectively, compared to pristine GBGS in the air. Additionally, these gases can be detected in very low concentrations, such as 95.2 parts-per-trillion (ppt) for NO_2 and 59.9 ppb for NH_3 [12]. The enhanced sensing capabilities of doped GBGS indicate a potential for improving the detection of toxic gases and developing more efficient GBGSs.

Hybridisation is another method that bases the combination of graphene with other materials such as polymers, nanoparticles or metal-oxides. Such systems can improve the sensing properties of graphene by providing additional active sites or increasing the surface area. J. Ma and others increased the NO_2 sensitivity of the pristine GBGS 13 times higher. PG/defective graphene (DGr) hybrid structure has been achieved by creating defects on PG by implementing silicon ion (Si^+) irradiation and controlling the defect size by altering the H_2 etching process time under the 300 ℃ annealing temperature [13]. B. Cho et al. created a nanoparticle/graphene hybrid gas sensor to enhance the NO_2 and NH_3 sensing properties. They reported that while the aluminium (Al) nanoparticles increased the NO_2 sensitivity, palladium (Pd) nanoparticles decreased the NO_2 sensitivity of the sensor. Modifying the sensor with Al nanoparticles resulted in a higher sensitivity to NO_2 gas due to the depletion of hole carriers. Conversely, the presence of Pd nanoparticles led to increased sensitivity to NH_3 gas by promoting the accumulation of hole carriers. The alteration of the electronic structure of a gas sensor resulting in varying sensitivity and selectivity characteristics is attributed to the distinct doping effects of metal nanoparticles. Therefore, it is crucial to evaluate the impact of each metal nanoparticle separately instead of generalising the concept of a high adsorption area [14].

Thermal annealing is another method to alter the surface structure of the GBGSs. Several studies have aimed to increase the sensing characteristic of the GBGSs by increasing the surface's activation of the adsorption sites after the annealing treatment. ZH. Ni and others have demonstrated that vacuum annealing of the GBGSs in different temperatures can increase the doping concentration by three orders of magnitude compared to non-annealed GBGS exposed to

ambient air. Different annealing temperatures can readily adjust the doping concentration, providing valuable insights into the impact of annealing on the properties of graphene [15]. Another research has demonstrated the annealing effect on the sensing properties of GBGSs. Rapid thermal annealing for one minute at 300 ℃ increased the sensitivity of GBGS to NO_2 gas concentration of 1 ppm, four times higher than the nonannealed pristine GBGS. Moreover, the atomic force microscopy (AFM) topographic images showed PMMA residues due to the CVD production of graphene having decreased ~4 times while surface roughness decreased ~3 times, indicating the surface cleaning effect of the annealing [16].

The photoactivation of graphene and other metal oxide (MOX)-based gas sensors have been previously studied and have demonstrated significant improvements in sensitivity, speed, and selectivity at room temperature [17]. Due to light illumination, the surface carrier density of the sensing material is altered, and the cleaning effect takes place through the activation of additional adsorption areas by removing passivating gases such as oxygen (O_2) and H_2O molecules from the sensing surface. Such photoinduced desorption of oxygen and water molecules creates additional adsorption sites on the p-doped GBGS, which decrease the current, which can take tens of hours to recover after turning off the illumination [18-20]. Therefore, with ultraviolet (UV) light treatment, sensor sensitivity and recovery can be increased.

2.3 Metal Oxide Functionalisation of the Graphene-based Gas Sensors

Metal oxide materials have gained widespread use in gas sensor applications due to their diverse and unique electronic structure, surface state, and morphology, which facilitate the detection of adsorbed gases on their surface by altering their resistivity. This property makes them suitable for detecting combustible, reducing, and oxidising gases. The high sensitivity and rapid response times of metal oxides to targeted gases and their low cost and compatibility with other structures make them ideal materials for detecting toxic and environmentally hazardous gases [21,22]. However, the high operating temperature of MOX sensors restricts their usage due to high power consumption [23]. Therefore, various studies have combined the superior properties of metal oxide materials with graphene to achieve better sensitivity, response, recovery, and lower operating temperatures [24]. This combination has exhibited a large specific surface area with numerous active sites for the adsorbed gases on the surface. Also, most metal oxides are n-type semiconductors, while graphene is a p-type semiconductor. The p-n junction that forms during the

integration process of the two materials can enhance the conductivity, which is explained through the phenomenon of the p-n heterostructure theory [25]. Kodu et al. succeeded in producing highly sensitive NO_2 sensors by functionalising the first GBGS with ZrO_2 and the second with silver (Ag), using the PLD (pulsed laser deposition) method. ZrO_2 functionalisation on graphene increased the NO_2 sensitivity by over 10 times compared to PG under 1 ppm NO_2 gas concentration at room temperature in synthetic air. Under UV excitation, the NO_2 sensitivity was approximately 40 times greater than that of PG. The SEM image in *Fig.* 2.1 shows the porous granular structure of ZrO_2 and small clustered Ag after the deposition of 2850 pulses of ZrO_2 and 720 pulses of Ag [26]. Several other studies have demonstrated that the functionalisation of GBGS with metal oxide materials can increase their sensitivity, selectivity, response, and recovery compared to pristine GBGS, although the specific techniques used for functionalisation may vary [18, 27, 28].

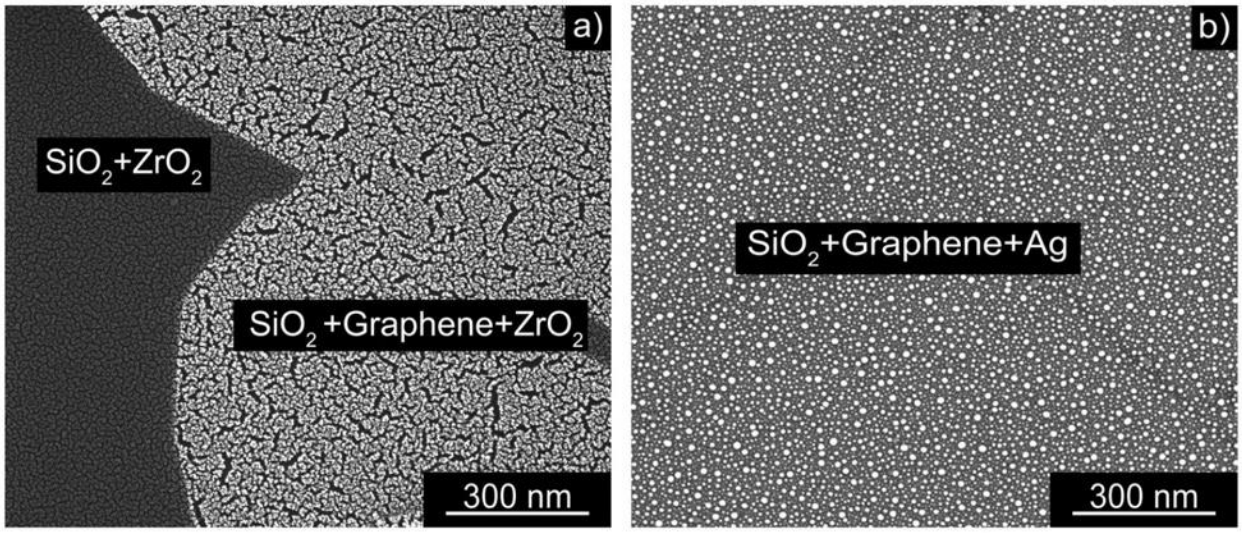

Fig. 2.1:SEM images of graphene sensors with pulsed laser-deposited ZrO_2 (a) and Ag (b). Adapted from [26].

2.4 Laser-induced Forward Transfer (LIFT)

Although laser printing was studied as early as the late 1960s, the term "LIFT" was first used by Bohandy et al. in their study on laser-induced transferring of copper (Cu) patterns onto a silicon substrate in 1986 [29]. Since then, LIFT has gained significant attention for research interests. LIFT is a digital printing technique that uses pulsed laser beams to transfer thin film materials from a donor to a receiving substrate. The donor material typically consists of a transparent substance, such as glass, quartz or fused silica, which allows the laser beam to pass through. This donor material is coated with the material intended for transfer. Each pulsed laser beam ejects the material from the donor and propels it toward the receiving substrate due to the adsorbed laser beam energy. The transfer mechanism may vary depending on several factors, including the thin film materials utilised, the physical state of the thin films (solid or liquid) and the specific LIFT method employed. Compared to the LIFT method, screen printing and photolithography require unique elements like screens or preexisting patterned masks for each copy, which can result in a high fixed cost and inflexibility. Inkjet printing and aerosol jet printing require a nozzle for printing, which is limited by the rheological properties of the ink and printable viscosity values are limited. However, LIFT, as a nozzle-free digital printing technique, provides more flexibility and cost-effectiveness in addition to its ability to print various materials with high precision, resolution and writing speed that can be achieved with the help of computer-controlled systems to create 2D or 3D complex patterns consisting of individual “voxels” [30]. The simplified transfer process of the LIFT method can be seen in *Fig.* 2.2.

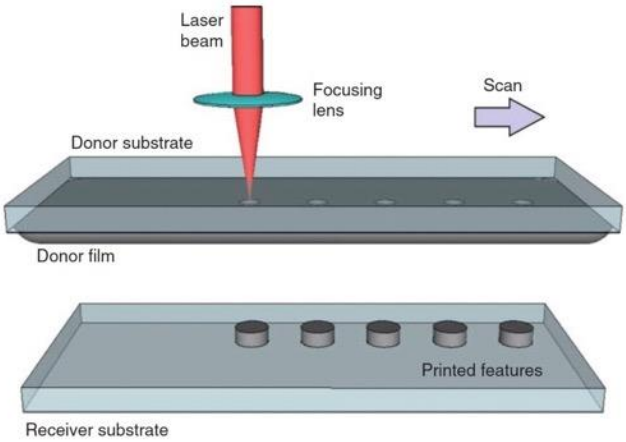

Fig. 2.2: The operation principle of the LIFT technique. Adapted from [31].

In recent years, there has been a notable improvement in the LIFT's ability to transfer thin film materials. A recent study demonstrated that it is possible to perform the LIFT of very thin materials, such as graphene [32]. The researchers in this study utilised a triazene-based polymer as a "dynamic release layer", which is capable of absorbing UV light, decomposing, and releasing N_2 gas as a thrust gas to propel the layer for transfer. Additionally, the dynamic release layer offers UV light protection for the material to be transferred. Prior to the LIFT process, graphene films were produced via CVD on a copper foil and subsequently transferred onto a quartz substrate coated with a release layer using a PMMA film. This coated quartz substrate served as the donor substrate for the LIFT process. After the transfer process, Raman spectroscopy was performed on the transferred graphene area of the receiver substrate. The results showed strong peaks at 1580 cm^{-1} and 2690 cm^{-1}, corresponding to G and 2D peaks. These peaks are indicative of a single layer of graphene. Although the authors reported that the substrate mostly consisted of single-layer graphene, no data on the D peak was provided, which strongly correlates with graphene defects and can be used to determine the number of graphene layers [33]. The LIFT method, as previously explained, has been successful in transferring various 2D or 3D thin film materials, including but not limited to single-walled carbon nanotubes [34], graphene oxide [35], metals (Al) [36] and metal-oxides (ZrO_2) [37]. This success showcases the robustness, accuracy, and efficiency of the LIFT technique, which enables non-destructive and precise material transfer.

2.5 Blister-Based Laser-induced Forward Transfer (BB-LIFT)

Numerous versions of the LIFT technique exist, each with distinct methods for absorbing and transforming the laser energy into mechanical energy to transfer the intended material [29]. However, certain transfer methods are more advantageous for biomaterials, thermally sensitive, or fragile materials, as direct laser ablation can cause inevitable damage. Although the conventional LIFT method is capable of transferring materials such as graphene or carbon nanotubes, as previously mentioned, the production process involves several transfer steps containing chemical treatments that can result in undesired residues, defects and intrinsic electronic and optical damages after the transfer. In recent years, a novel LIFT variation called BB-LIFT has been proposed to address these issues. Instead of using a polymer-based dynamic release layer, a thin metal layer described as a "carrier-sacrificial film donor layer" is employed to absorb the laser beam and form a "blister" formation between the metal/glass interface that propels the material

coated above it. One key difference between the conventional LIFT and the BB-LIFT methods is that while the former requires a laser fluence above the threshold for successful transfer of the thin metal layer to the receiver substrate, the latter should not exceed the threshold but instead must be marginally lower to induce the formation of a bulge or blister. It is noteworthy that exceeding the threshold may contaminate the transferred material with the carrier-sacrificial film donor layer [38]. A schematic diagram illustrating the difference between LIFT and BB-LIFT is presented in *Fig.* 2.3.

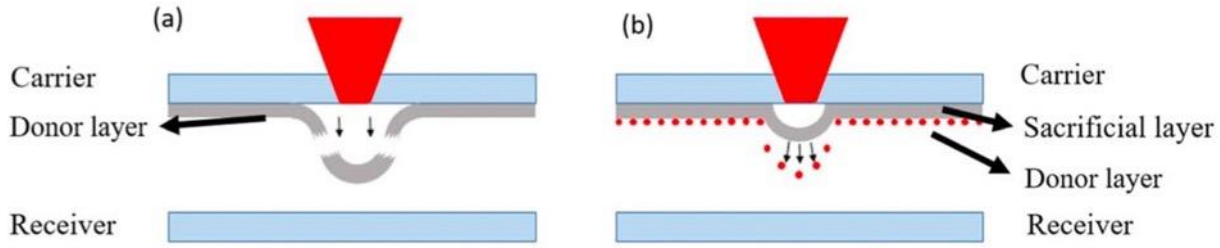

Fig. 2.3: Schematic representation of two variations of the LIFT process. Typically, a transparent carrier material such as quartz or fused silica is utilised to facilitate the passage of the pulsed laser beam. The traditional LIFT process, depicted in (a), involves the transfer of a metal film as donor material through the shock generated by the pulsed laser. The BB-LIFT process, illustrated in (b), utilises the metal film as a sacrificial layer. The donor film is coated with thermosensitive material, which can be propelled towards the receiver by the laser-induced deformation of the sacrificial film. Adapted from [38].

According to NT Goodfriend [39], two proposed explanations exist for the blister formation mechanism in BB-LIFT. The first explanation suggests that blister formation is caused by the ablation between the carrier material, such as glass, quartz or fused silica, and the thin metal film due to the pulsed laser beam. This ablation generates a confined plasma plume that creates the necessary pressure to expand the thin film, resulting in the propelling of the donor layer. The second explanation proposes that the blister is formed due to the thermal expansion of the thin metal film. As the metal film cannot expand into the glass substrate or laterally due to the confinement of the temperature gradient, it expands perpendicular to the glass substrate to form the blister. The author notes that for the high-pressure ablation mechanism, the ductility of the thin metal film and the ablation threshold are the primary parameters that affect blister formation. However, for the thermal expansion mechanism, the malleability and thermal expansion coefficient of the thin metal film are the crucial parameters that influence blister formation.

To investigate the two interpreted ideas, Goodfriend conducted several experiments using both femtosecond and nanosecond lasers. It was theorised that the pulse duration significantly affects the material being impacted due to the interactions between electrons and lattice. Electrons have a higher velocity and operate on a shorter timescale, while nuclei are relatively stationary and operate on a longer timescale. When photons are absorbed by electrons, the energy is transferred to nuclei on a picosecond timescale, and heat transfer via nucleic vibrations takes place on a nanosecond timescale. A femtosecond pulse will impart all its energy to the electrons, reducing their energy level without the chance to transfer it to the lattice, whereas the electrons under the nanosecond pulse will transfer energy to the lattice in a far shorter timeframe than nanoseconds, resulting in a steady build-up of lattice vibrational energy.

Based on the experimental results obtained, the author indicated that the observed phenomena depend on the duration of the pulsed laser beam employed. The experimental findings align with the theoretical proposition that the utilisation of a nanosecond laser beam produces expansion in accordance with the thermal expansion coefficient of the thin metal layer. Conversely, employment of a femtosecond laser causes ablation and a resultant phase change in the thin film metal, leading to gas expansion and the formation of blisters that correspond to Young's modulus of the thin layer metal. An illustration of these outcomes is depicted in *Fig.* 2.4.

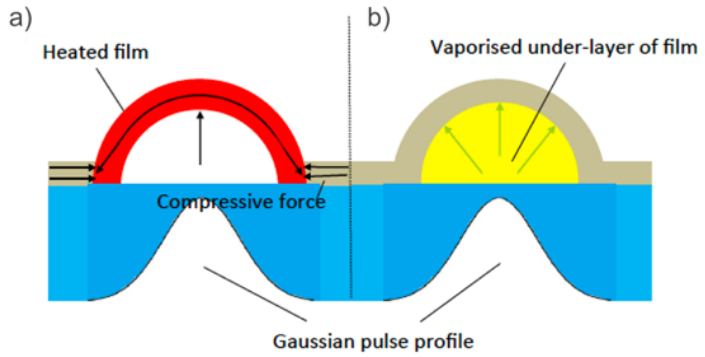

Fig. 2.4: Illustration of the blister formation mechanism. (a) ns incident pulse. As the film gets heated, it undergoes expansion, which causes the projection of both the film and particles in a direction perpendicular to the substrate. (b) fs incident pulse. The film experiences ablation at its interface with the substrate, resulting in the generation of a trapped plasma/gas. The expansion of this plasma/gas causes the stretching of the film, which ultimately leads to the formation of the blister. Vertical dimensions are exaggerated for illustration and not to scale. Reproduced from [39].

Previously, BB-LIFT transfer of 2D molybdenum disulfide (MoS_2) and molybdenum diselenide ($MoSe_2$) [39], organic compound (porphyrin) [40], luminescent diamond nanoparticles [41], diamond nanopowders [42], single-wall carbon nanotubes [43] and CVD graphene [44] have been demonstrated. Therefore, it is evident that the BB-LIFT technique is robust in its ability to transfer a variety of fragile and organic materials without the need for additional chemical treatments. This can be accomplished cleanly and without causing any damage to the transferred material.

3. Materials and Method

3.1 Sample Preparation

The LIFT requires the preparation of two distinct substrates: the donor and the receiver substrates. The donor substrate is composed of the material intended for transfer and a carrier sacrificial layer, typically made of metal, which is required to generate the blistering effect for transfer. As a donor substrate base, a transparent material is employed to facilitate UV light transmission. For the present investigation, both sides of polished fused silica (MaTecK, 10x10x1 mm^3) were utilised for each donor substrate due to its high UV transmission properties.

On the other hand, the receiver substrates were used to serve as receivers for the transferred materials in the LIFT process. In this study, the typical Si/SiO_2 wafers (10x10x0.5 mm^3, 25 nm SiO_2, thermally grown, MTI Corporation) and graphene sensors were used as receiver substrates. All donor and receiver substrates were meticulously prepared by Dr Tauno Kahro and Dr Margus Kodu in the laboratories of the Institute of Physics at the University of Tartu, as described in Ref. [45].

3.1.1 Preparation of Donor Samples

To prepare the donor substrates, a rigorous surface cleaning process was conducted on the fused silica wafers to eliminate any organic and inorganic impurities. This involved treatment with piranha solution at 80°C for 5 minutes, followed by ultrasonic cleaning with distilled water for 5 minutes. The wafer was subsequently cleaned with RCA-1 solution at 80 °C for 10 minutes and rinsed again with ultrasonic distilled water for 5 minutes. This was followed by cleaning with RCA-2 solution at 80°C for 10 minutes and a final rinse with ultrasonic distilled water for 5 minutes to complete the surface cleaning process.

The cleansed wafers were then coated with a chromium (Cr) layer (nominally 4 nm) layer via electron beam deposition (EBD), followed by the deposition of a 1410 nm layer of Al using thermal evaporation. The Cr layer was applied onto the fused silica wafer prior to the Al layer due to prevent the Al layer from peeling off in the water during the graphene/PMMA transfer. Later, the typical graphene (LG Corporation)/PMMA transfer onto the Al layer was conducted. Then, the PMMA layer was removed with a dichloromethane solution. Later, pulsed laser deposition (PLD) was employed to deposit ZrO_2 thin films on donor substrates. A KrF laser (248 nm, 25 ns pulse

duration) with an energy density of 3 J/cm^2 was used for ablation on a ceramic ZrO_2 target. The other deposition parameters were as follows: the distance between the substrate and target was 75 mm, the O_2 pressure during deposition was 10^{-1} mBar, the laser pulse repetition rate was 5 Hz, and the substrate temperature was at room temperature. Before deposition in a PLD chamber under vacuum conditions held at room temperature, the donor substrates were heated for 1.5 hours at 150°C. The obtained base pressure was $>2x10^{-6}$ mBar before starting the deposition. The approximate growth rate was known from previous work, and it was used to deposit ZrO_2 films with nominal thicknesses of 0.5 nm, 5 nm, and 50 nm. *Fig.* 3.1 illustrates the prepared graphene donor substrate after the LIFT.

Fig. 3.1: Photograph of Si/SiO_2 substrate (above) and graphene-coated donor substrate (below).

3.1.2 Preparation of Receiver Substrates

The cleaning procedures employed for the fused silica substrates were similarly applied to the Si/SiO_2 wafers. The Si/SiO_2 wafers were thoroughly cleansed and coated with CVD graphene/PMMA. The same PMMA removal process was then repeated. Afterwards, Ti (4nm) / Au (60nm) electrodes were deposited on the graphene-coated wafers, producing graphene sensors as receiver substrates. These sensors were later cleaved, yielding four sensors in each piece. *Fig.* 3.2 illustrates the prepared graphene sensors. To conduct accurate NO_2 electrical gas sensing measurements of each sensor, it was necessary to isolate them, as multiple sensors were located on a single substrate. In this regard, the electrical separation of the sensors (electrode pairs) was

achieved by employing a nanosecond pulse laser (Horus Laser HLX-I-F020) to cut the graphene material.

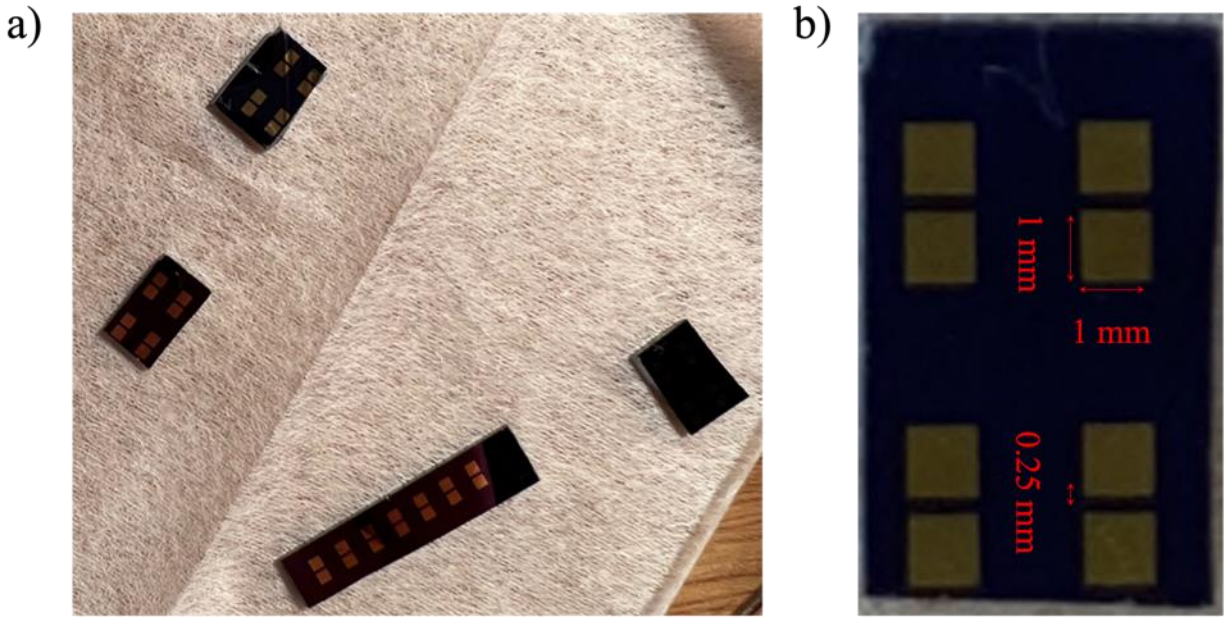

Fig. 3.2: Photograph of (a) cleaved graphene sensors before the LIFT and (b) a receiver substrate consisting of 4 sensors.

Overall, all prepared donor and receiver substrates can be listed as follows:

Donor Substrates:

1. SiO_2/Cr/Al
2. SiO_2/Cr/Al/Gr
3. SiO_2/Cr/Al/Gr/ZrO_2 (0.5 nm)
4. SiO_2/Cr/Al/Gr/ZrO_2 (5 nm)
5. SiO_2/Cr/Al/Gr/ZrO_2 (50 nm)
6. SiO_2/Cr/Al/ZrO_2(50 nm)

Receiver Substrates:

1. Si/SiO_2
2. Si/SiO_2/Gr/Au (electrodes)

3.2 BB-LIFT Experiment Setup

The BB-LIFT experiments were conducted using a KrF (krypton fluoride) excimer laser (Coherent COMPexPro 205, wavelength 248 nm, pulse duration 25 ns). The pulse energy was set to 200 mJ, the voltage was maintained at approximately 20 kV, and the repetition rate was set to 1 Hz for all experiments. Subsequently, the generated UV light was focused through the samples using optical mirrors and lenses. The energy of the laser impulses arriving on the sample was regulated by manually adjustable laser beam energy attenuator optics.

The attenuated laser beam energy was measured using a laser power/energy meter (Ophir Nova II). Due to the use of a high-energy excimer laser, a pyroelectric energy sensor was employed for pulse energy measurement through the beam splitter in attenuation mode (7.9%). This pulsed energy measurement setup demonstrated the total energy of the pulsed beam, while only 7.9% of the laser beam energy was reflected onto the pyroelectric energy sensor due to the beam splitter. This setup was necessary to protect the pyroelectric energy sensor from direct irradiation by the excimer laser, which could easily damage it.

Subsequently, a beam blocker was used to control the pulsed laser beams, which were manually moved to allow the laser beam to pass onto the samples. Then, the pulsed laser beams were irradiated onto the manual XY stage. The donor and receiver samples were placed on a 10x10mm platform positioned in the centre of an XY stage to achieve control over the pulsed laser beam locations. A sheet metal with a 10x10mm hole was mounted onto the XY stage using bolts to ensure that the samples remained in place without any movement during the experiment. A mask was used to ensure that the laser beam spots were uniformly distributed in size and energy, with a circled hole with a diameter of 1.5 mm drilled into the sheet metal and aligned with the laser beam. The positions of the laser beams were measured using two rulers, one on the x-axis and the other on the y-axis, with a 1 mm margin of error. Finally, a red laser diode with an adjustable laser spot diameter was used, aligned with the UV laser beam, to enable precise adjustment of the XY stage so that the desired transfer location on the substrates and the excimer laser focus would coincide, thereby providing complete control over the intended laser beam hit spots. *Fig.* 3.3 depicts the schematic of the BB-LIFT experimental setup.

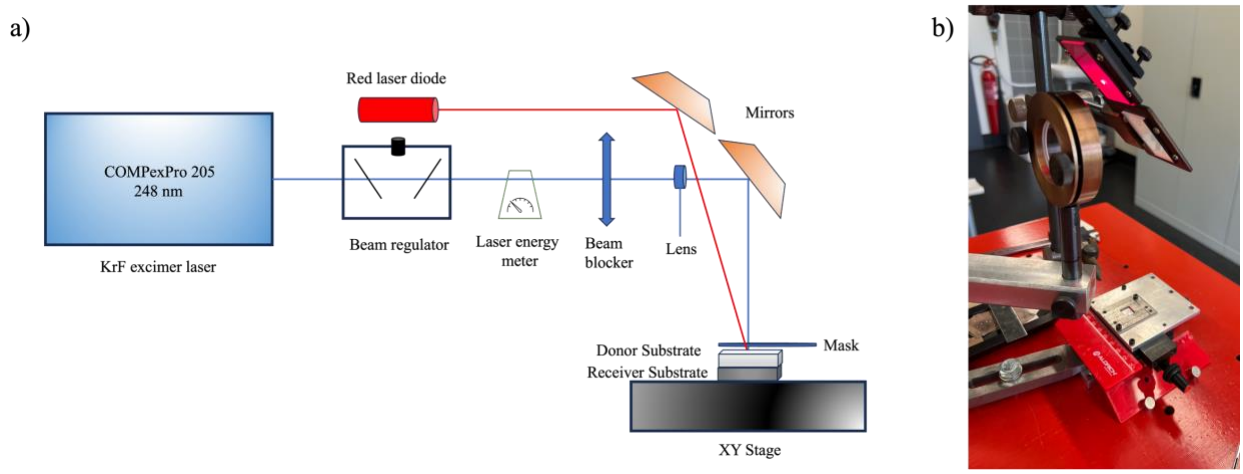

Fig. 3.3: (a) Schematic of the blister-based LIFT experiment setup. (b) Photograph of optical mirrors, lenses and XY stage.

Several parameters control the BB-LIFT transfer mechanism, and one of these parameters is fluence (F) in J/cm^2, which is defined as the amount of energy delivered per unit area by the pulsed laser beam and can be expressed mathematically as follows:

$$\text{Fluence } \left[\frac{\text{Joules}}{\text{cm}^2}\right] = \frac{\text{Laser pulse energy [J]}}{\text{Effective focal spot area [cm}^2\text{]}}, \qquad (3.1)$$

For the LIFT process, it is essential to determine the optimal fluences that can result in the blister formation of the thin metal layer and allow the transfer of the coated material onto the receiver substrate. Higher fluences provide more energy to the metal layer, resulting in its transfer by melting, while lower fluences do not transfer sufficient energy for blister formation on the thin metal layer, thereby preventing the intended material's transfer. Accordingly, several fluences were employed to obtain the most efficient transfer of the intended materials onto the receiver substrate, using graphene and Al-coated donors, followed by an optical microscope and Raman spectroscopy analysis of both receiver and donor substrates to confirm the transfer of the intended material. Subsequently, the optimal fluences were determined and employed for the LIFT of graphene sensors.

To utilise Equation *(3.1)*, the effective focal spot area was determined by directing pulsed laser beams onto UV-sensitive paper positioned on the XY stage. The exposed area on the paper was then measured using a calliper (~ 0.072 cm²). The laser pulse energy was adjusted and measured

using manually adjustable beam attenuation optics and a laser power/energy meter (Ophir Nova II). However, since the laser beam experiences energy losses after transmission through the optics and mirrors, the energy loss factor, R, was calculated by determining the energy difference of the laser beam before and after transmission onto the sample surface, resulting in a value of 0.82. The Equation *(3.1)* was then adjusted as follows:

$$\text{Fluence } \left[\frac{\text{Joules}}{\text{cm}^2}\right] = \frac{\text{Laser pulse energy [J]} \times \text{Energy loss factor (R)}}{\text{Effective focal spot area [cm}^2\text{]}}, \qquad (3.2)$$

During experimentation to determine the optimal fluence for the LIFT, a range of fluences (F=0.2, 0.35, 0.5, 0.6, 0.72, 0.85, 1.0, 1.15, 1.25, 1.5, 1.7 J/cm^2) were selected. These values were then adapted to the aforementioned formula, and the necessary laser beam energies were calculated. The laser beam energies were subsequently regulated and measured using the manually adjustable beam displacement optics and the laser energy meter (Ophir Nova II).

Optimum fluences were then employed in the LIFT, where the laser beams were precisely targeted between the Au electrodes using sheet metal with a 1.5 mm diameter circled hole aligned with the donor sample and by adjusting the laser beam location with a manual XY stage and rulers.

As demonstrated by a previous study [44], the space between the donor and the receiver substrates during the LIFT of CVD graphene can cause uneven and excessive dispersion of the transferred material, thus leading to imprecise results. Therefore, in this study, the donor and receiver substrates were brought into contact to achieve precise transfer of the material onto the GBGSs.

3.3 Electrical Gas Sensing Measurement Setup

Two different gas measurement setups have been utilised, each with slight differences in their systems. As previously described in detail [20], a gas mixture was created by passing cylinder gases through mass flow controllers and into a mixer. The LIFTed and annealed sensors were placed in a test chamber with 100 cm^3 internal volumes. The total gas flow rate through the chamber remained constant at 200 sccm (standard cubic centimetre per minute), while the flow rates of individual gases (N_2, O_2, N_2/H_2O, and N_2/NO_2 mixture) were manipulated by mass flow controllers (Brooks, SLA5820). The gases employed in the study were 99.999% pure (AS Linde). To sustain synthetic air conditions throughout the measurement, O_2 gas flow was maintained at 21% while the relative humidity of the testing gas was sustained at 50% by introducing a portion

of the N_2 flow into a water bubbler and the gas pressure in the test chamber was maintained at atmospheric pressure. The gas flow composition was controlled using LABVIEW-based software. The resistances of the LIFTed GBGSs were recorded, with a sampling rate of once per second, using a custom-built data acquisition system based on the Arduino NANO microprocessor and 12-bit A/D converters. On the other hand, the gas sensitivity measurements of the annealed sensors were performed using sourcemeters (Keithley 2400, 2450, and 7001) and switchbox Keithley 7001. Both configurations allowed for measuring 4 sensors simultaneously. The applied voltage between the graphene sensor electrodes was maintained at 100 mV. In addition to this setup, a multimeter was utilised to measure the sensitivity of the sensors before and after the LIFT. For measurements under light excitation, the Thorlabs LED (365 nm wavelength) and Xenon/Mercury lamp (Hamamatsu) were used with a light intensity of approximately 10 mJ/cm^2 on the graphene sensors.

3.4 Characterisation Setups

The characterisation of samples used for the LIFT can provide valuable information about their surface chemistry and structure. Therefore, in this study, the surface structure of donor and receiver substrates was investigated using several characterisation techniques. An optical microscope was utilised to observe changes on the donor and receiver substrate surfaces after the LIFT, utilising different magnifications. Raman spectroscopy (Renishaw, inVia, excitation wavelength 514 nm, spot size ~ 1 μm, 10% incident power) was employed to detect graphene on both the donor and receiver substrate surfaces, both before and after the LIFT, to assess the transfer of graphene and ZrO_2. Finally, SEM (FEI Nova NanoSEM 450) was used to visualise the graphene, Al, ZrO_2, and remaining surface structure of the donor and receiver substrates.

4. Results and Discussion

4.1 LIFT on Si/SiO_2 Receiver Substrates

Prior to the LIFT of graphene sensors, it was crucial to determine the optimum fluences for the LIFT. Hence, Si/SiO_2 wafers were employed as the receiver substrates, which were observed after the LIFT process.

4.1.1 LIFT with SiO_2/Al Donor Substrate

This study utilised a thin Al layer as the carrier-sacrificial film donor layer, which absorbed the pulsed laser beam energy, leading to blister formation and subsequent material transfer. Thus, the LIFT process was anticipated to propel the transferred material exclusively, not the thin Al layer, as the latter could contaminate the receiver substrate by leaving Al residues. Consequently, donors were LIFTed with F=1.0, F=1.25, and F=1.5 J/cm^2 fluences. *Fig.* 4.1 illustrates the optical microscope images of donor and receiver substrates LIFTed with various fluences.

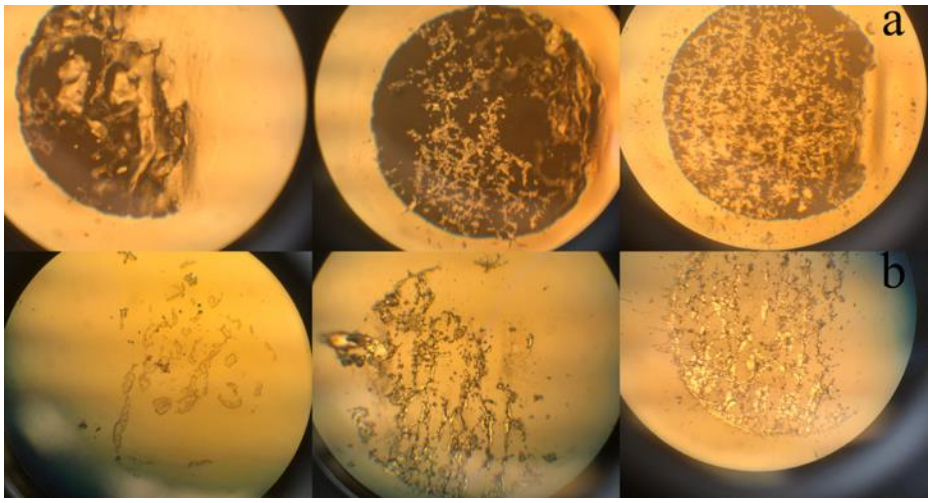

Fig. 4.1: Optical microscope images of SiO_2/Al Donor and Si/SiO_2 receiver substrates in reflection mode after the LIFT: (a) donor substrates LIFTed with F=1.0, F=1.25, and F=1.5 J/cm^2 fluences from left to right respectively, (b) and corresponding receiver substrates aligned in the same order.

As depicted in *Fig.* 4.1, all receiver substrates LIFTed above the F=1 J/cm^2 fluences contained Al residues. The density of transferred Al augmented as the fluences increased towards F=1.5 J/cm^2. Hence, the optimum fluence should remain below F=1.0 J/cm^2, where the Al layer will not transfer but merely create the blister formation.

4.1.2 LIFT with SiO_2/Cr/Al/Gr Donor Substrate

The graphene-coated donor substrate was used to LIFT graphene onto the Si/SiO_2 receiver substrate. For this purpose, a range of fluences, namely F=0.5, F=0.6, F=0.72, F=0.85, F=1.0, F=1.25 and F=1.5 J/cm^2, were employed. Although previous experience indicated that the presence of Al residues could be observed above the F=1.0 J/cm^2 fluence, a wide range of fluences were tested for the sake of clarity, as the donor substrate used here was from a different batch. *Fig.* 4.2 illustrates the optical microscope images of the donor and receiver substrates LIFTed with various fluences.

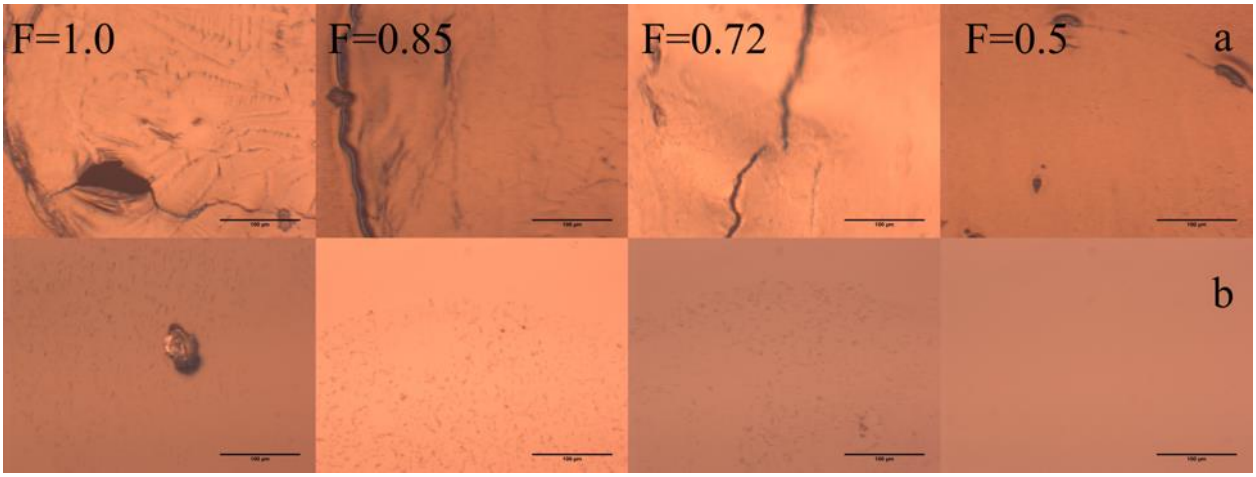

Fig. 4.2: Optical microscope images of the SiO_2/Cr/Al/Gr donor and Si/SiO_2 receiver in reflection mode after the LIFT, showing the edge of the transferred areas. (a) Donor substrates with respective fluences, (b) Corresponding receiver substrates aligned in the same order. The image scale is 100 µm.

In *Fig.* 4.2, circular shapes were observed at the edge of the receiver substrates corresponding to the region where LIFT occurred. No Al residues were observed on the receiver substrates that were LIFTed below the F=1.0 J/cm^2 fluence. In contrast, only a small amount of Al residues were found on the receiver substrate LIFTed with the F=1.0 J/cm^{2}fluence.

Furthermore, optical microscope images taken from the edge of the LIFTed locations of the receiver substrate revealed the presence of “micron-sized islands” that appeared as black dots on the image, later identified as "graphene flakes." These islands were densely distributed on the receiver substrate that was LIFTed with F=1.0, F=0.85, and F=0.72 J/cm^2 fluences, suggesting that these fluences could be good candidates for further LIFT experiments. Additionally, on the donor

substrates, after the pulsed laser beams, fractural lines were observed, more prominently on the donor substrates that were LIFTed with F=0.85 and F=0.72 J/cm^2 fluences due to the thermal expansion mechanism [39].

Raman spectroscopy, a commonly used technique for characterising graphene and other carbon materials, was employed to investigate the LIFTed regions of the Si/SiO_2 receiver substrate to determine whether the graphene was successfully transferred via LIFT. *Fig. 4.3* presents the Raman spectra of the micron-sized islands on the Si/SiO_2 receiver substrate after the LIFT with various fluences, along with the Raman spectra of PG obtained from the previously mentioned graphene source (LG) on the Si/SiO_2 substrate for the comparison.

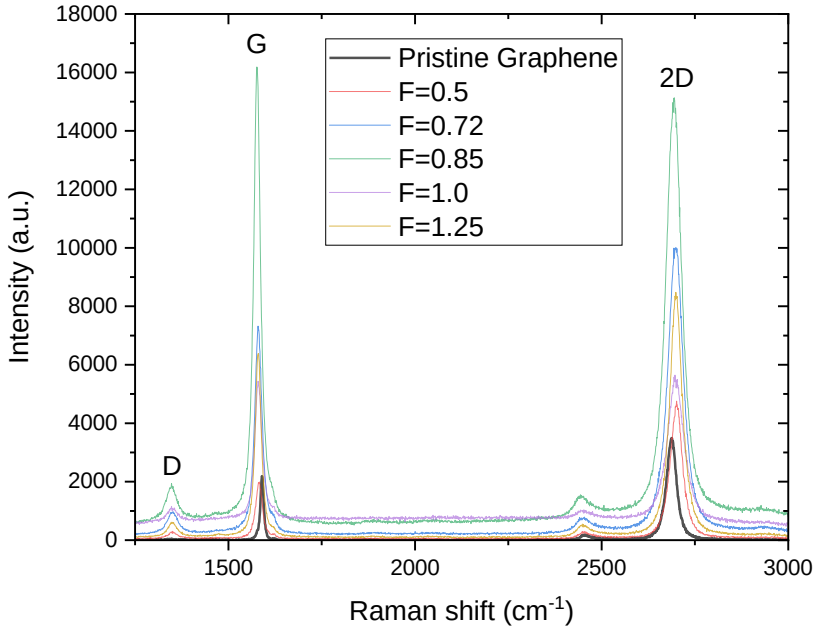

Fig. 4.3: The Raman spectra of pristine graphene and the micron-sized islands on the Si/SiO_2 receiver substrate LIFTed via various fluences.

All LIFTed spots of the receiver substrate using various fluences and PG exhibited typical Raman spectra of graphene, characterised by strong 2D (2690 cm^{-1}) and G (1580 cm^{-1}) band peaks [32]. The notable D (1350 cm^{-1}) band peaks of the LIFTed graphene, compared to PG, suggest that the LIFTed graphene is more defective. The 2D band shift of the LIFTed graphene towards the higher wavenumber indicates the presence of multilayer graphene. The peak intensity ratio, which is the ratio of the 2D and G peak intensities, I_{2D}/I_G, is another indicator for detecting multilayer graphene. The peak intensity ratios of graphene for LIFTed F=0.5, F=0.72, F=0.85, F=1.0, F=1.25 J/cm^2

fluences and PG are 2.4, 1.35, 0.93, 1.03, 1.3, and 1.6, respectively. A higher intensity ratio indicates single-layer graphene, while a lower intensity ratio indicates bilayer or multilayer graphene, as reported in Ref [33].

Although the small number of graphene flakes at the spot LIFTed with F=0.5 J/cm^2 fluence made it difficult to observe with the optical microscope, the highest intensity ratio was observed on this spot, indicating the single-layer graphene. Despite the initial single-layer configuration of the graphene material upon being transferred from the donor substrate using the LIFT process, the graphene experiences fragmentation and crumpling upon reaching the receiver substrate, attributable to the transfer mechanism. Consequently, the Raman spectra exhibit variations across different locations of the graphene flakes, influenced by the degree of crumpling and the number of layers that have formed.

4.2 LIFT on Graphene Sensors

4.2.1 LIFT with SiO_2/Cr/Al/Gr and SiO_2/Cr/Al/Gr/ZrO_2 (0.5 nm and 5 nm) Donor Substrates

In this experiment, the graphene sensors were LIFTed using various fluences with graphene and graphene + ZrO_2 (0.5 nm and 5 nm) coated donor samples and investigated through an optical microscope, Raman spectroscopy and SEM. Moreover, the impact of the LIFTed materials on NO_2 sensing was analysed via gas sensing measurement.

Previously cleaved graphene sensors were employed to conduct the investigation. One sensor from each substrate was reserved as a control group. The remaining three were LIFTed with graphene, graphene + 0.5 nm ZrO_2, and graphene + 5 nm ZrO_2, utilising SiO_2/Cr/Al/Gr and SiO_2/Cr/Al/Gr/ZrO_2 (0.5 and 5 nm) donor substrates, correspondingly. Different fluences (F=0.72, F=0.85, and F=1.0 J/cm^2) were utilised to LIFT each sensor group (between each pair of Au electrodes), while one pair of Au electrodes was not LIFTed for comparison. The utilisation of the F=0.5 fluence for the LIFT of graphene sensors was not feasible due to the low observed density of graphene flakes on the Si/SiO_2 sample.

Fig. 4.4 depicts optical microscope images (Renishaw inVia Raman microscope) of the LIFTed areas between the Au electrodes of each sensor before and after the LIFT, prior to the Raman spectroscopy measurement.

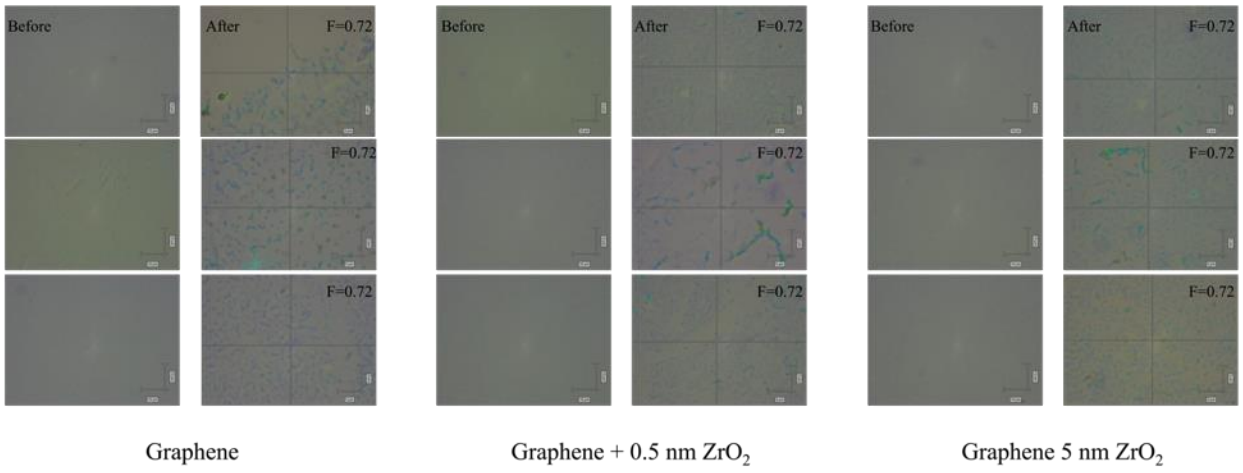

Fig. 4.4: Optical microscope images between the electrodes of the graphene sensors before and after the LIFT via different fluences, with graphene, graphene + 0.5 nm ZrO_2 and graphene + 5 nm ZrO_2. The optical microscope image scale is 5 μm.

The images above show that the graphene flakes were formed for all LIFTed areas of each sensor, similar to the optical microscope images taken from the graphene LIFTed Si/SiO_2 receiver substrate. The fourth sensor of each set was not LIFTed, and thus no optical microscope images were presented, as there were no observable changes.

It can be deduced that the sensors intended to be LIFTed with graphene + 0.5 nm ZrO_2 and graphene + 5 nm ZrO_2 were successfully transferred, as these ZrO_2 layers were coated on top of the graphene layers, and graphene flakes were formed on the sensors as a result of the LIFT. However, more conclusive results were obtained through the Raman spectroscopy data and SEM images.

To investigate the characteristics of the LIFTed materials on the graphene sensors surface, Raman spectroscopy measurements were performed between the electrodes of the sensor surfaces before LIFT and at the imaged areas presented in *Fig.* 4.4, which were located onto the micron-sized islands, after the LIFT. The Raman spectra of both sensors and donor samples are illustrated in *Fig.* 4.5.

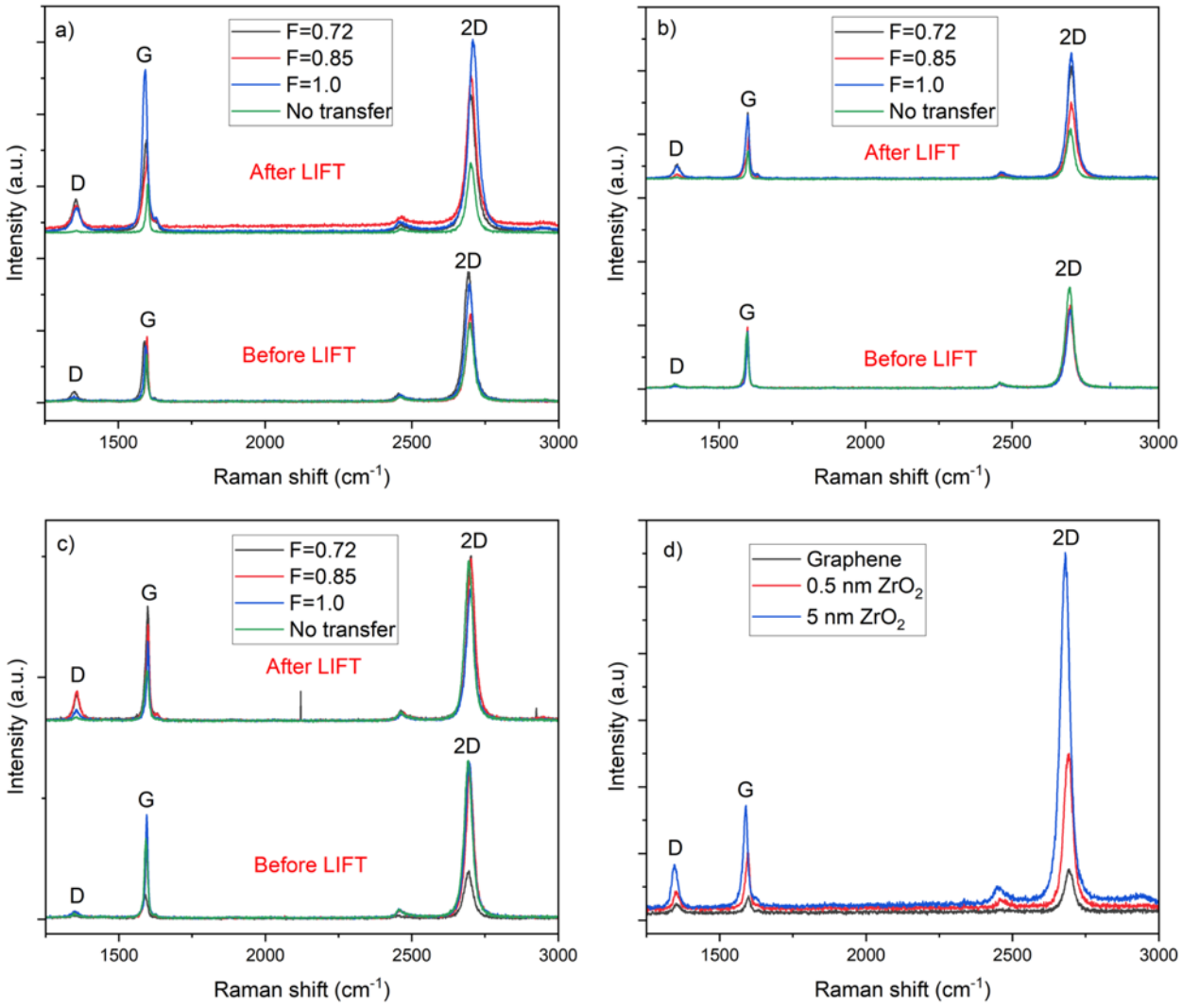

Fig. 4.5: Raman spectra between the electrodes of each graphene sensor before LIFT, and on the graphene flakes between the electrodes after the LIFT of (a) graphene, (b) graphene + 0.5 nm ZrO_2, and (c) graphene + 5 nm ZrO_2 via different fluences. (d) Raman spectra of donor substrates before the LIFT. "No transfer" refers to the Raman spectra of the control group of each sensor without LIFT.

As depicted in *Fig.* 4.5, the Raman spectroscopy of the micron-sized islands showed a significant increase in the D band for each graphene sensor at various fluences, indicating an increase in defective structure compared to the non-LIFTed sensors (No transfer), which maintained their D band peak intensity. Additionally, the I_{2D}/I_G peak intensity ratio indicated a significant decrease for the graphene LIFTed sensor at F=1.0 J/cm^2 fluence, compared to before the LIFT, indicating the formation of multilayer graphene. The Raman spectra of the donor samples exhibited strong 2D and G peaks of graphene, with the 5 nm ZrO_2-coated donor sample exhibiting the highest

defectiveness, followed by the 0.5 nm ZrO_2-coated donor sample and the graphene-coated sample having the least defectiveness, as observed from the intensity of their D band peak. It was deduced that the coating of ZrO_2 through PLD caused defectiveness on the graphene surface, possibly due to the extreme conditions during the PLD process [Kodu 2016]. The Raman spectroscopy measurements, along with the confirmation of the optical microscope images, provided evidence that the graphene was transferred from the donor substrates onto the graphene sensors.

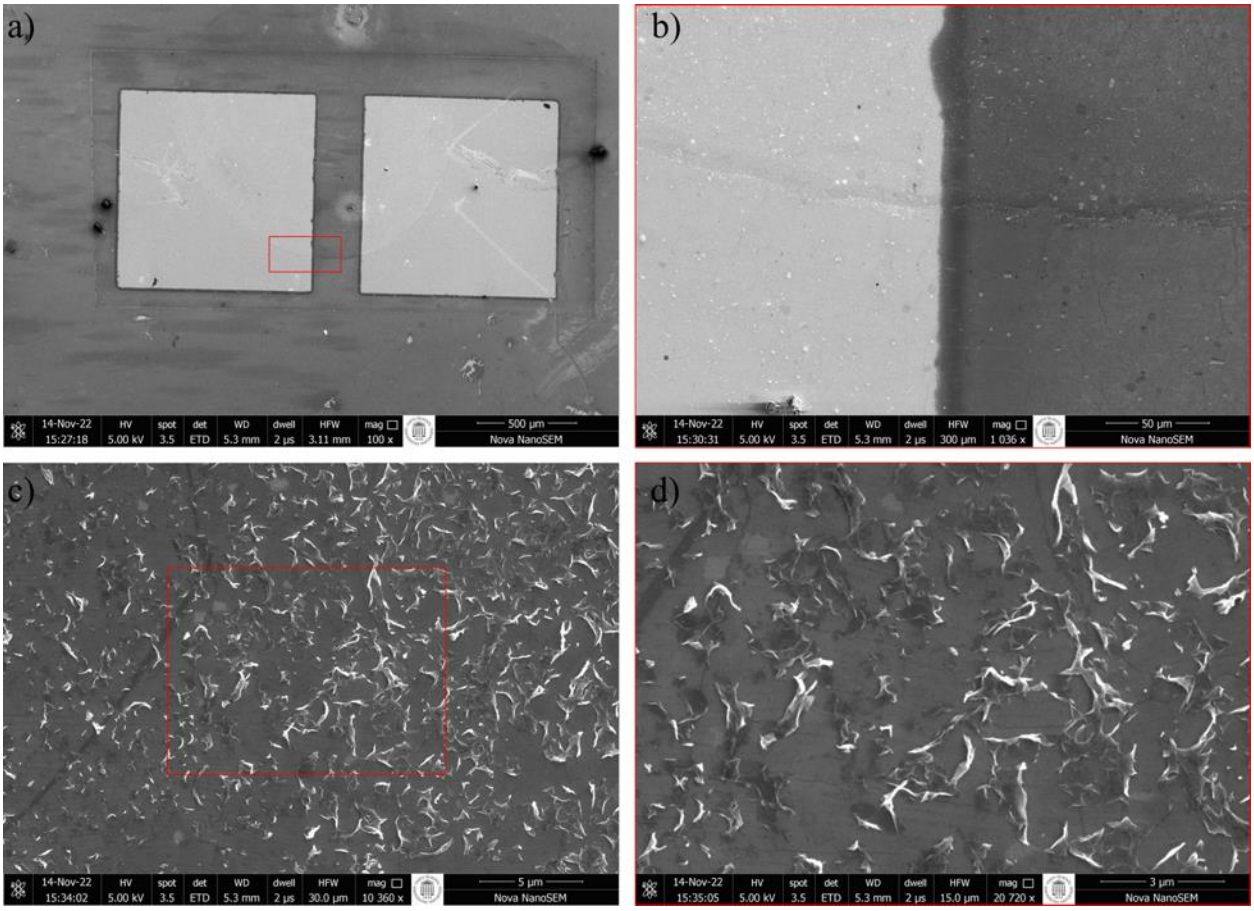

Fig. 4.6: SEM images of the graphene + 5 nm ZrO_2 LIFTed graphene sensor via F=0.85 J/cm^2 fluence. (a) The LIFTed area between the electrodes. (b) Magnified view of the red rectangle from (a), exhibiting an edge of the LIFTed area. (c) Densely distributed graphene flakes. (d) The magnified image of the red rectangle from (c) illustrates graphene flakes.

Fig. 4.6 depicts the graphene sensor underwent the LIFT via graphene + 5 nm ZrO_2 using F=0.85 J/cm^2 fluence. The laser cutting performed to separate each sensor for obtaining more precise results from the gas sensing measurements can be observed around the Au electrodes in *Fig.* 4.6

(a). Also, the circle formation represents the area that underwent LIFT. *Fig.* 4.6 *(b)* shows a magnified image of the edge of the LIFTed area. The difference in the surface structure is visible, with the non-LIFTed sensor surface exhibiting a smooth CVD graphene layer, whereas the graphene + 5 nm ZrO_2 LIFTed site shows micron islands composed of individually distributed "graphene flakes". The LIFT process, as evidenced by the crater formation shown in *Fig.* 4.6 *(c)*, produced a highly dense graphene-flake-contained region surrounding the crater. An enlarged image of the densely distributed graphene flakes is demonstrated in *Fig.* 4.6 *(d).*

SEM images of the graphene sensors subjected to LIFT of graphene via F=1.0 J/cm^2 fluence can be found in **Appendix A**. These images elucidate the impact of a higher fluence during LIFT. Notably, the circled formation depicted in *Fig.* 4.6 *(a)* exhibits reduced clarity due to the utilisation of a lower fluence. Similarly, *Fig.* 4.6 *(b)* demonstrates that the edge of the circled formation experienced less deterioration, aligning with the application of a lower fluence.

The SEM images of the LIFTed regions reveal the transfer of graphene as graphene flakes. Although it was presumed that the ZrO_2 layer, which was coated on top of the graphene layer on the donor sample, would also be transferred with the graphene, the thinness of the layer (0.5 and 5 nm) precluded its observation using the SEM device due to its technical limitations.

To comprehend the impact of LIFT with graphene and ZrO_2 materials on the graphene sensors, NO_2 sensing measurements were conducted on each group of LIFTed sensors. Furthermore, the resistance of each pair of sensors was evaluated in each sensor group before and after the LIFT, as well as after sensor separation by laser cutting via a multimeter. *Fig.* 4.7 illustrates the gas sensing measurement findings and the sensor resistance values obtained throughout the experimental procedure. The relative gas response is defined as a relative change in conductance, expressed by the following equation:

$$S=\frac{(G-G_0)}{G_0}\times 100\% , \tag{4.1}$$

where G represents the relative change in conductance, G_0 denotes the conductance in synthetic air, and S represents the gas response amplitude.

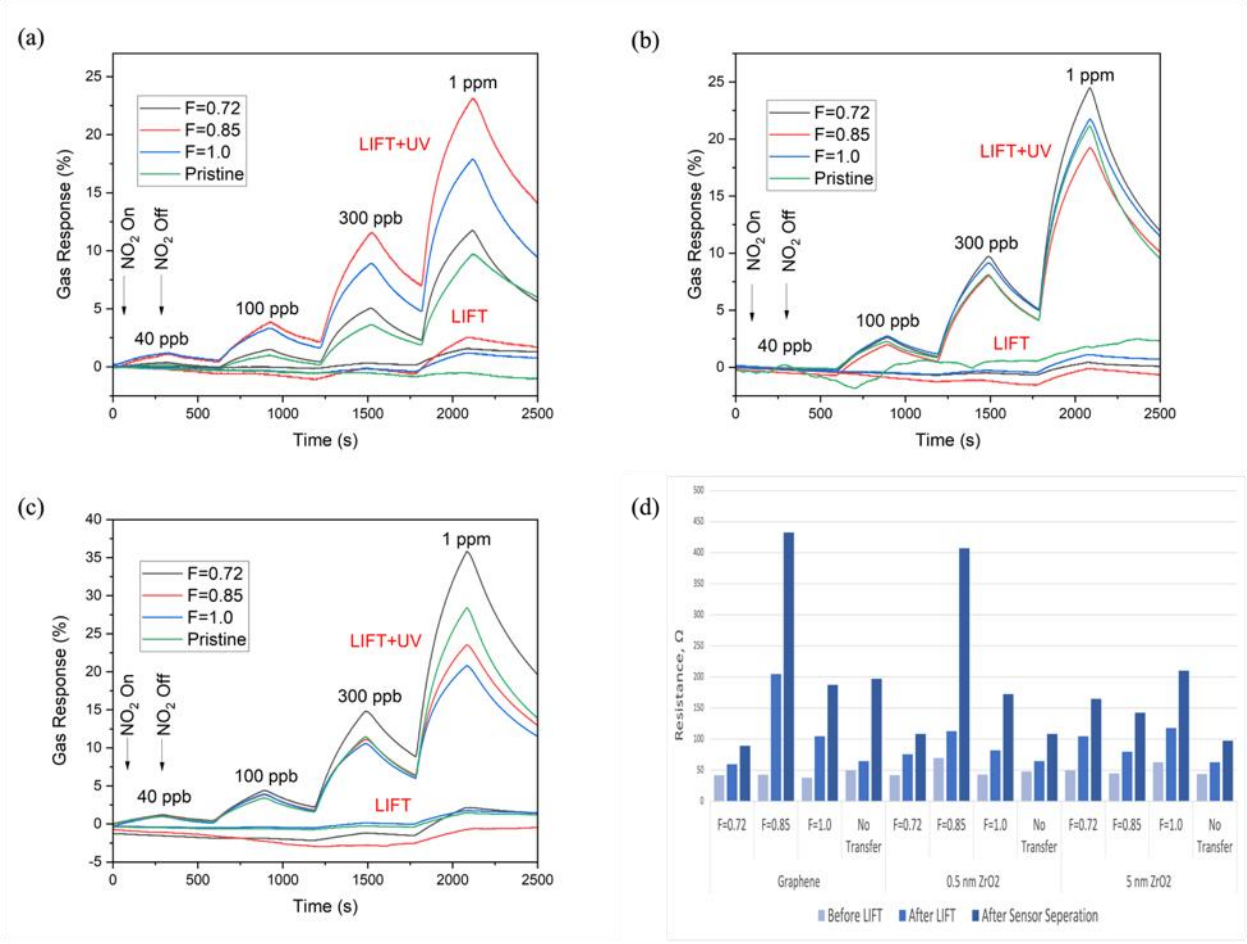

Fig. 4.7: The temporal responses to NO_2 with and without UV illumination at varying gas concentrations of the (a) graphene, (b) graphene + 0.5 nm ZrO_2, and (c) graphene + 5 nm ZrO_2 LIFTed graphene sensors via different fluences. (d) Resistance change in the graphene sensors before LIFT, after LIFT and after the sensor separation, in various fluences. "Pristine" refers to sensors without LIFT. The wavelength of UV light was 365 nm, and its intensity was ~10 mW/cm^2. Responses were recorded in dry air at room temperature (22 ℃).

The NO_2 sensing measurements of the LIFTed sensors exhibited a noticeable increase in sensitivity under UV light compared to the measurements conducted in the absence of light. This was attributed to the surface cleaning effects of UV light, which led to the creation of more adsorption sites for NO_2 molecules and a corresponding increase in current, indicating p-type doping of the LIFTed sensors and pristine graphene sensors.

The resistance of all sensors increased after LIFT, with even the pristine graphene sensors displaying a relatively low increase in resistance compared to the LIFTed sensors. After sensor

separation, the resistance increased for both LIFTed and pristine graphene sensors, with a dramatic increase observed for graphene LIFTed and graphene + 0.5 nm ZrO_2 LIFTed sensors via F=0.85 J/cm^2 fluence. This increase in resistance after the LIFT was expected due to the alteration in surface structure caused by the transferred material, while the increase in resistance after sensor separation was anticipated due to the limited conductive area after the separation.

Although a significant increase in sensitivity of the graphene sensors after the LIFT could not be observed compared to the pristine graphene sensor, this behaviour was associated with the LIFTed graphene, as the ZrO_2 clusters were concealed inside the graphene flakes, thereby impeding their interaction with the sensor surface, resulting in less improvement in NO_2 sensing than expected. An alternative explanation is that the thickness of the ZrO_2 layers coated was not adequate to cause a substantial increase in sensing on the sensor surface.

To investigate the obtained results, further gas-sensing experiments were conducted using donor substrates coated with a thicker (50 nm) ZrO_2 layer and coated with the same thickness of ZrO_2 but without a graphene layer between the Al and ZrO_2 layer to investigate the effect of the graphene release layer.

4.2.2 LIFT with SiO_2/Cr/Al/ZrO_2 (50 nm) and SiO_2/Cr/Al/Gr/ZrO_2 (50 nm) Donor Substrates

Considering the preceded gas sensing measurements, alternative donor samples were utilised to investigate the effect of varying thicknesses of the transferred material on NO_2 gas sensing. Specifically, one donor sample was coated with 50 nm ZrO_2 on top of graphene, while another was coated with 50 nm ZrO_2 on top of Al to employ them for the LIFT on graphene sensors and subsequently compare the results. This approach was undertaken to assess the impact of the thicker ZrO_2 layer and graphene release layer on the ZrO_2 surface distribution on the graphene sensors.

The optical microscope images illustrate the LIFTed region of each sensor before and after the LIFT, prior to the subsequent Raman spectroscopy analysis, as presented in **Appendix B**. The findings indicated that the graphene sensors subjected to LIFT using a graphene + 50 nm ZrO_2 donor substrate exhibited surface characteristics containing graphene flakes, consistent with previous results. In contrast, the surface structures of sensors treated solely with a 50 nm ZrO_2 layer, without graphene, remained unaltered.

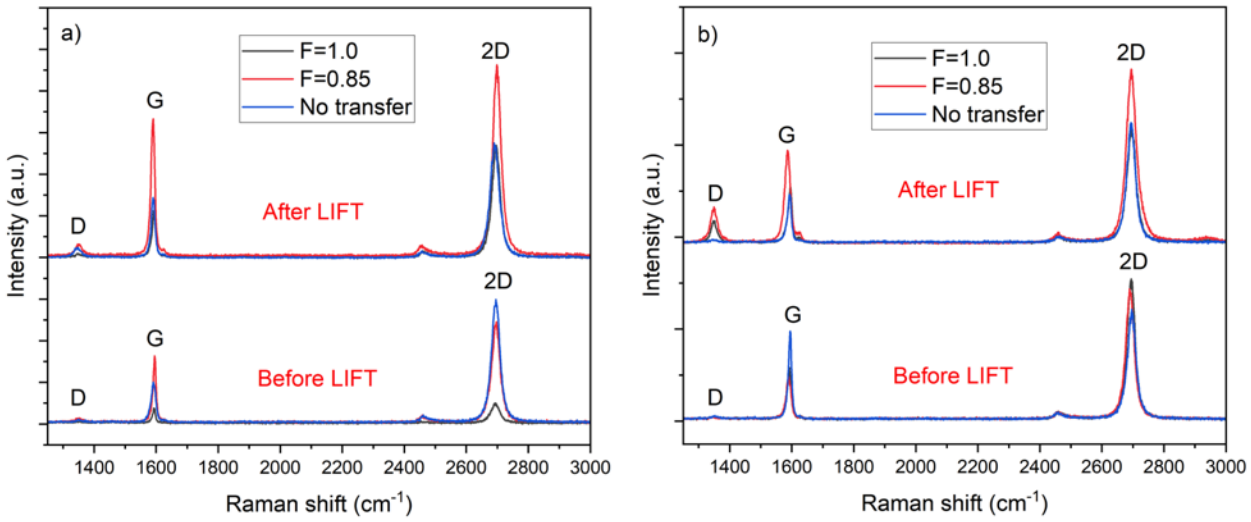

Fig. 4.8: Raman spectra between the electrodes of each graphene sensor before LIFT, and on the LIFTed regions/graphene flakes between the electrodes after the LIFT of (a) 50 nm ZrO_2 and (b) graphene + 50 nm ZrO_2 via different fluences. "No transfer" refers to the Raman spectra of the control group of each sensor without LIFT.

As illustrated in *Fig.* 4.8, the sensors subjected to LIFT at varying fluences exhibited an increase in the intensity of the characteristic D peak. Notably, the sensors LIFTed with graphene + 50 nm ZrO_2 donor demonstrated a higher D peak intensity than those treated with only a 50 nm ZrO_2 donor. This observation implies that the inclusion of graphene in the LIFT results in the formation of a more defective structure.

SEM images of the graphene + 50 nm ZrO_2 LIFTed graphene sensors via F=1.0 and F=0.85 J/cm^2 are depicted in *Fig.* 4.9 *(a)* and *(b)*, respectively. The presence of ZrO_2 can be observed as unevenly dispersed particles of varying sizes in both images. *Fig.* 4.9 *(a)* displays a region where the ZrO_2 layer was transferred as a homogeneous sheet, while *Fig.* 4.9 *(b)* shows a graphene flake surrounded by ZrO_2 clusters. Some ZrO_2 clusters are trapped within the graphene flakes, while others have adhered to the flakes. Additionally, the remaining clusters are distributed across the sensor surface in diverse sizes. A comparison of these images with *Fig.* 4.6 *(d)*, where graphene flakes were distributed, reveals that the ZrO_2 clusters are more prominently visible in *Fig.* 4.9, likely due to the utilisation of larger-sized ZrO_2 clusters. The presence of clusters with varying sizes in the distribution can be attributed to the fragile structure of the thin ZrO_2 layer. When the pulsed laser beam impacts the Al layer, the ductile nature of the Al layer allows it to form blisters due to thermal

expansion. However, the ZrO_2 layer exhibited no deformation or elongation in response to the Al blister formation. Instead, the ZrO_2 layer underwent fracturing, resulting in fragmented propulsion and the creation of micron-sized fragments rather than a contiguous thin sheet on the graphene sensor surface. A similar distribution pattern is observed for graphene, as it also transfers as graphene flakes, being an atomically thin and fragile material. However, one could speculate that in regions where the donor and receiver substrates come into atomic-level contact, the ZrO_2 layer is transferred as a thin sheet, where graphene acts as a web or adhesion layer, facilitating the bonding of the ZrO_2 layer and promotes the formation of a continuous structure rather than fragmentation as illustrated in *Fig.* 4.9 *(a)*.

On the other hand, the graphene sensors that were subjected to LIFT using solely 50 nm ZrO_2, without the inclusion of a graphene release layer as shown in *Fig.* 4.10, did not exhibit any observable presence of ZrO_2 or similar structures, unlike the graphene sensors LIFTed with graphene + 50 nm ZrO_2. This observation highlights the crucial role of the graphene release layer in the LIFT process. The graphene release layer contribution to the blistering effect is essential for facilitating the transfer of ZrO_2 clusters. In contrast, when the Al layer was used without graphene, the transfer of ZrO_2 did not occur. This outcome can be attributed to the stronger bonding between the Al and ZrO_2 layers, which hinders the successful transfer of ZrO_2 clusters.

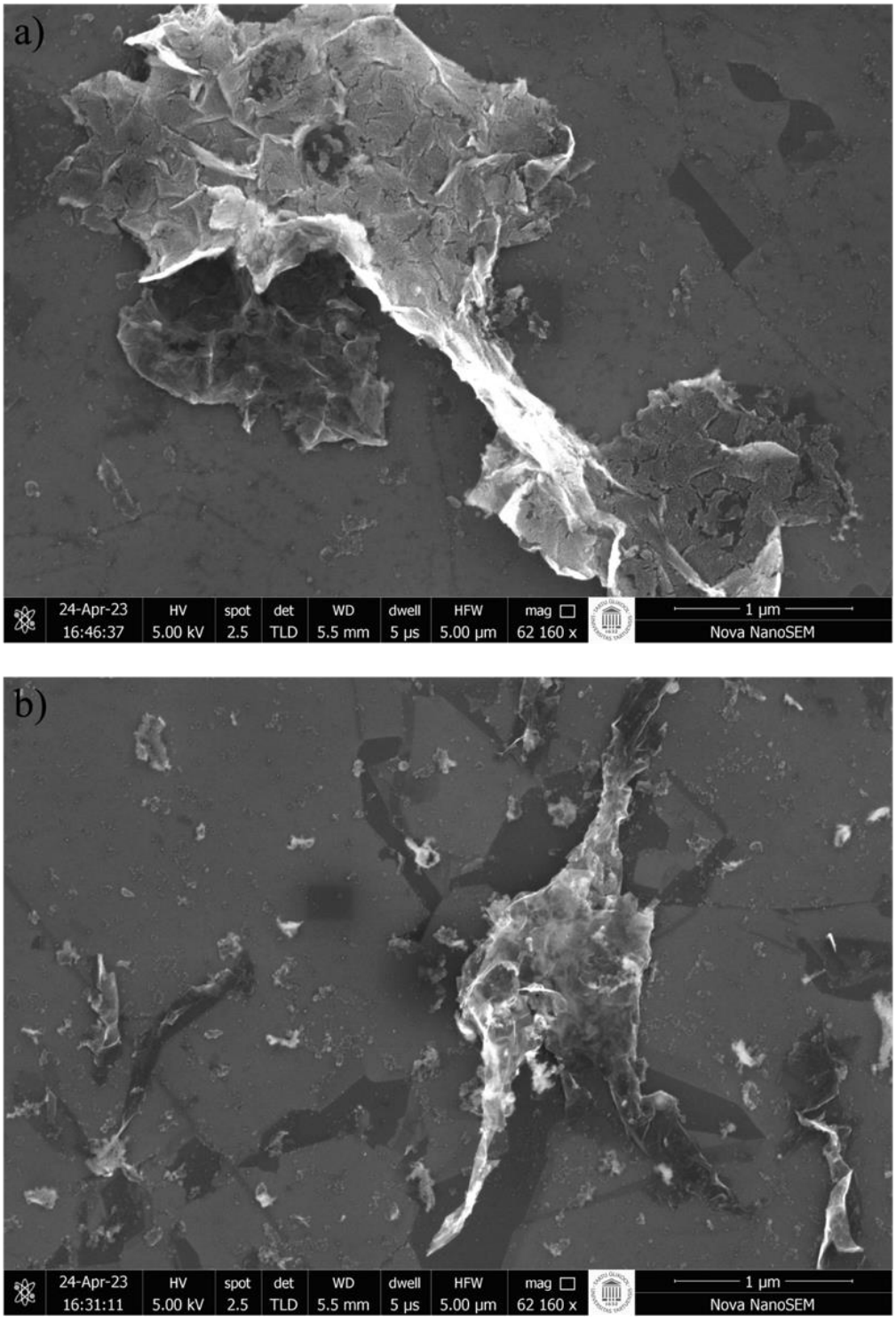

Fig. 4.9: SEM images between the electrodes of the graphene sensors, LIFTed with graphene + 50 nm ZrO_2 via (a) F=1.0 and (b) F=0.85 J/cm^2 fluences.

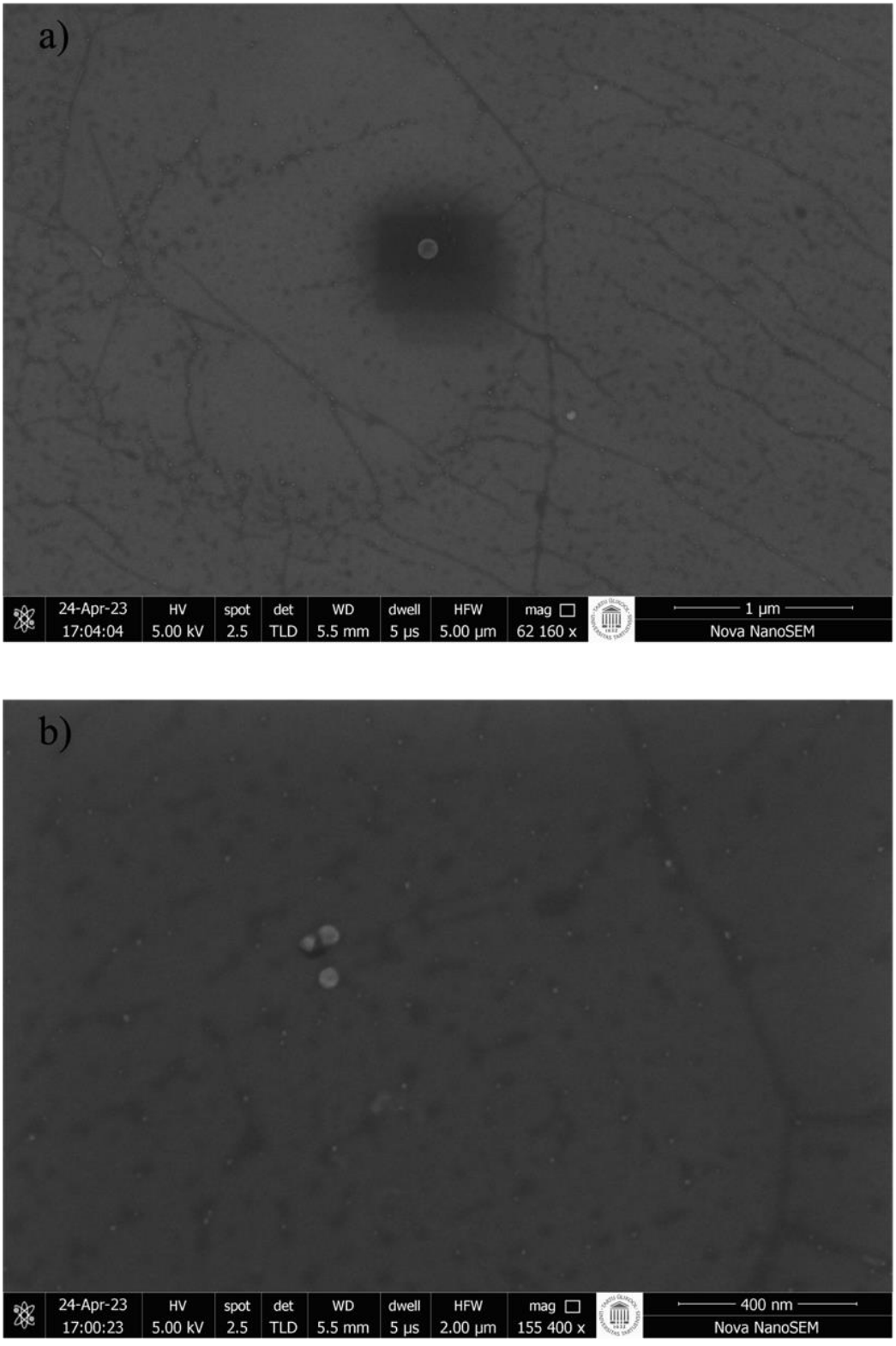

Fig. 4.10: SEM images between the electrodes of the graphene gas sensors, LIFTed with 50 nm ZrO2 via (a) F=1.0 and (b) F=0.85 J/cm2 fluences.

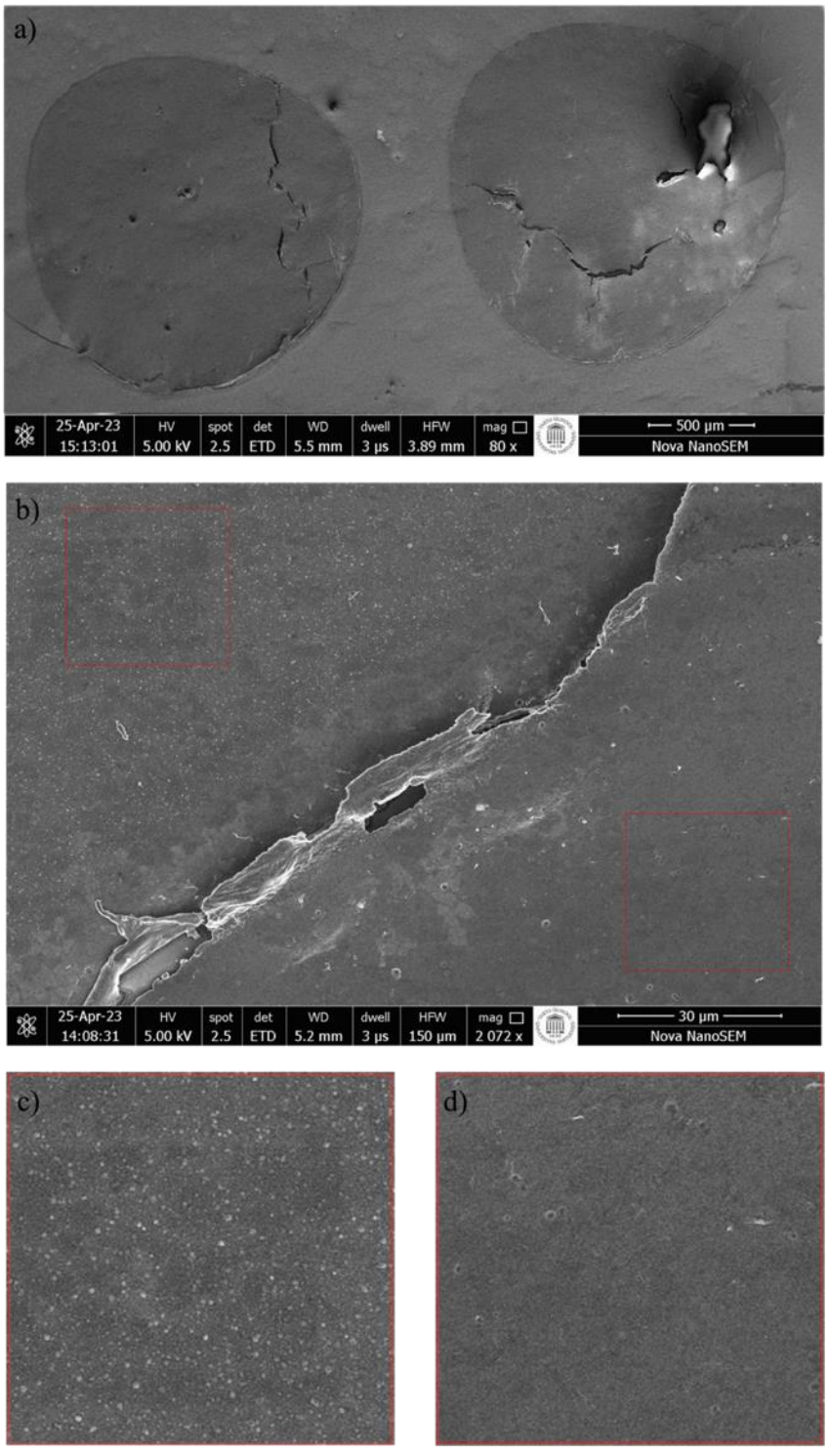

Fig. 4.11: SEM images of the donor substrate coated with graphene + 50 nm ZrO_2. (a) The regions LIFTed via F=1.0 and F=0.85 J/cm^2 fluences, represented on the left and right spots, respectively. (b) Close-up of the F=1.0 J/cm^2 LIFTed area's edge. Enhanced view of the red rectangles (30 x 30 µm) situated outside the LIFTed region (c) and within the LIFTed region (d).

Fig. 4.11 presents SEM images of the donor substrate, which was coated with graphene + 50 nm ZrO_2. In *Fig.* 4.11 *(a)*, the circled spots demonstrate a contrast difference, highlighting the region where the LIFT occurred. *Fig.* 4.11 *(b)* provides a more detailed depiction of the LIFTed and the non-LIFTed areas from the edge where the LIFT occurred. Magnified views of this region can be observed in *Fig.* 4.11 *(c)* and *(d)*, where the noticeable dissimilarities strongly indicate the successful transfer of ZrO_2 from the donor substrates. These SEM images establish a correlation and provide supporting evidence for the findings obtained from the graphene sensors, as depicted in *Fig.* 4.9, confirming the occurrence of ZrO_2 transfer.

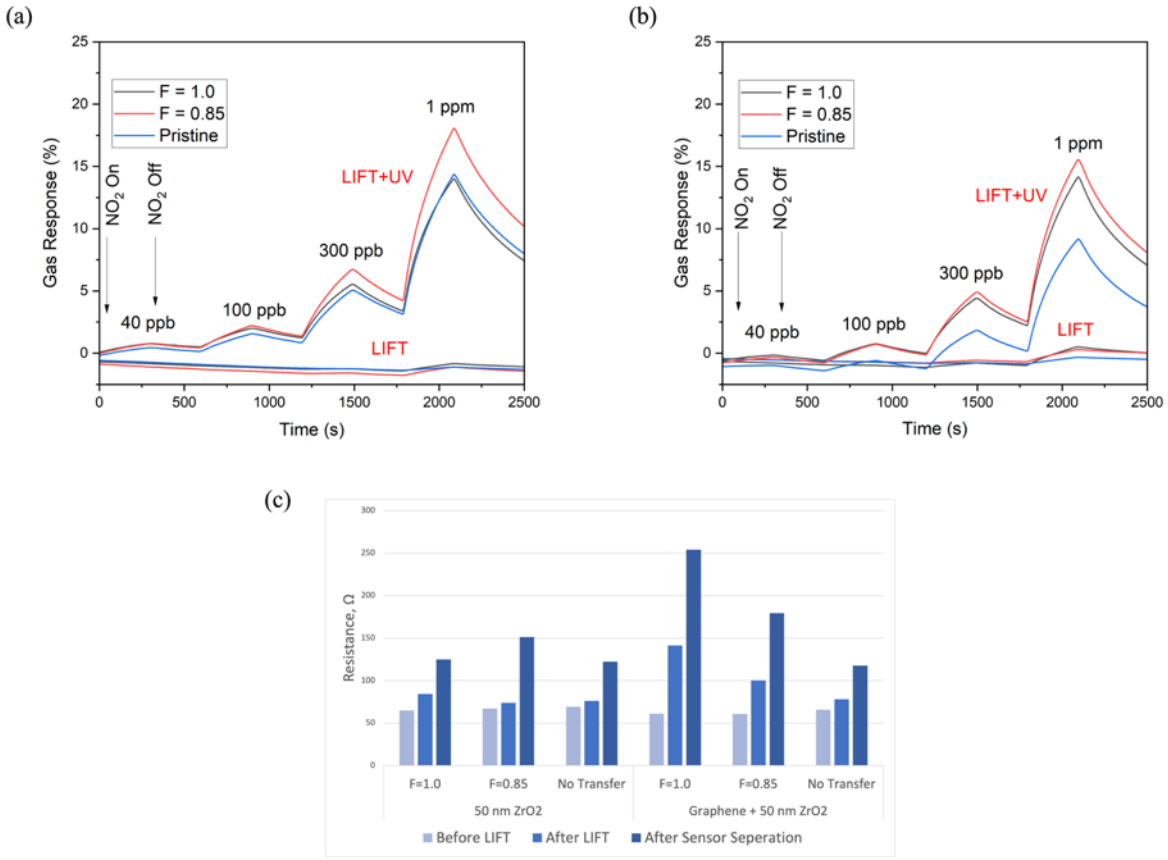

Fig. 4.12: Temporal responses to NO_2 with and without the UV illumination at various gas concentrations of the (a) 50 nm ZrO_2 and (b) graphene + 50 nm ZrO_2 LIFTed graphene sensors via different fluences. (c) The resistance change in the graphene sensors before, after LIFT and after the sensor separation, in various fluences. "Pristine" refers to sensors without LIFT. The wavelength of UV light was 365 nm, and its intensity was ~10 mW/cm^2. Responses were recorded in dry air at room temperature (22 ℃).

The findings from the NO_2 sensing responses conducted under the UV illumination, as depicted in *Fig.* 4.12 *(a)* and *(b)*, revealed that LIFT with F=0.85 J/cm^2 fluence resulted in the highest response for graphene sensors LIFTed with 50 nm ZrO_2 and graphene + ZrO_2. Specifically, the response values were approximately 4% and 8% higher than the pristine graphene sensors for 1 ppm concentration. Conversely, in the absence of UV illumination, both groups of sensors exhibited relatively weak sensitivity. Furthermore, the measured sensor resistances before and after the LIFT and after sensor separation showed a trend similar to that observed in the previous NO_2 gas sensing measurements, wherein each structural modification increased resistance on each sensor group.

The gas sensing measurements did not reveal a significant disparity in the NO_2 sensing capabilities between the graphene sensors LIFTed with 50 nm ZrO_2 and those LIFTed with graphene + 50 nm ZrO_2, nor when compared to the pristine graphene sensors. However, the SEM images presented above illustrate that the ZrO_2 layer was transferred in a distributed manner in the case of sensors LIFTed with graphene + 50 nm ZrO_2. It has been theorised that the primary factor contributing to the absence of significant NO_2 sensing was attributed to the limited energy available for the substitution of the transferred material into the adsorption sites on the surface of GBGS. Consequently, the micron-sized ZrO_2 clusters LIFTed onto the sensor surface exhibited a suspended state, as they merely hung on the surface without actively engaging with the adsorption sites through interaction.

4.3 Thermal Annealing of Graphene Sensors

Thermal annealing is a reliable post-treatment technique that can enhance the gas-sensing properties of graphene sensors by activating the adsorption sites present on the sensor surfaces. To this end, the graphene + 5 nm ZrO_2 LIFTed sensors used in the previous experiment were annealed at 500 ℃ for 3 hours in a 10^{-5} mbar setting using a PLD chamber. Following this, Raman spectra and gas sensing measurements were conducted to assess the impact of thermal annealing on the graphene structure and sensor characteristics.

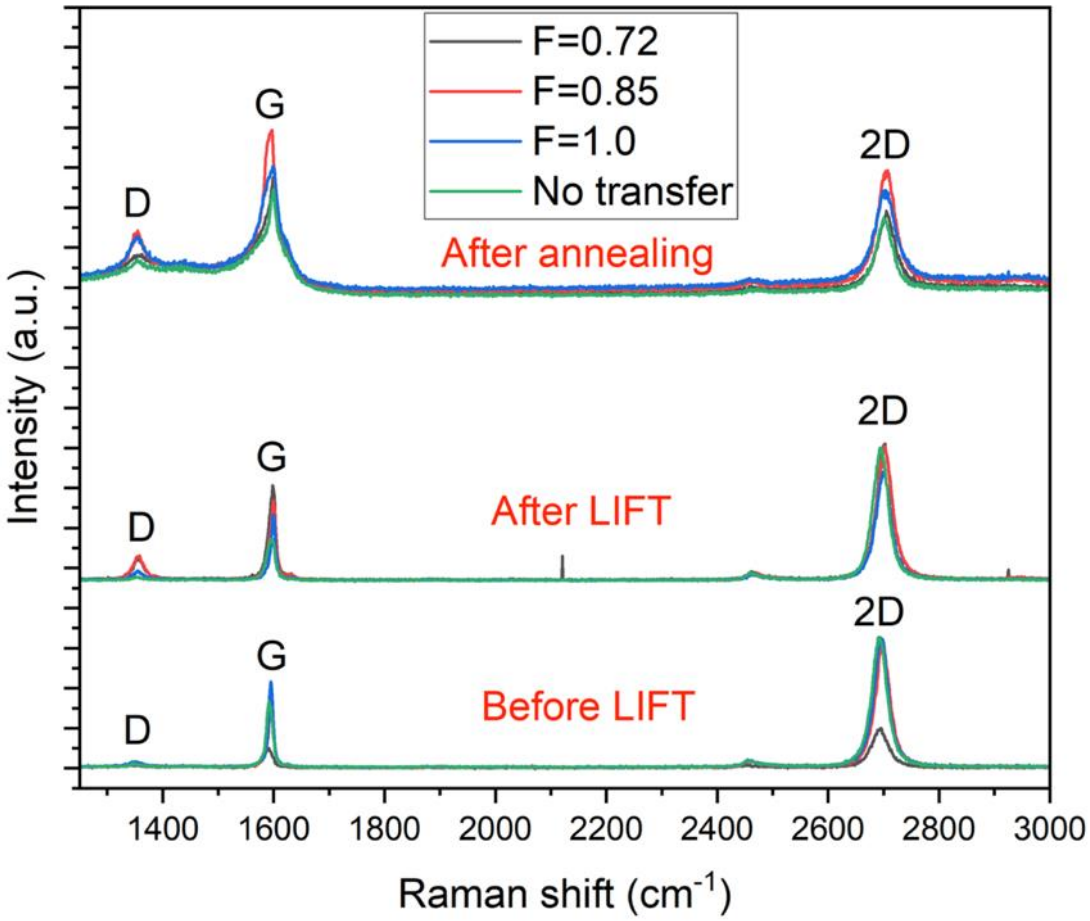

Fig. 4.13: Raman spectra between the electrodes of each graphene sensor before LIFT and on the graphene flakes between the electrodes after the LIFT of graphene + 5 nm ZrO_2 via different fluences, in addition to the Raman spectra of the graphene flakes after the thermal annealing. "No transfer" refers to the Raman spectra of the control group of each sensor without LIFT.

Fig. 4.13 reveals that the Raman spectra of the annealed sensor exhibited an increase in the characteristic D peak intensity and width, indicating the graphene's defectiveness on the sensor surface. Additionally, the $I_{2D}/_G$ intensity ratio was significantly decreased for all sensors following annealing, indicating the formation of crumpled graphene. Furthermore, a significant shift towards higher intensity between the G and D bands was observed, corresponding to the thermal annealing effect, which has also been reported in previous studies (Ref [16]).

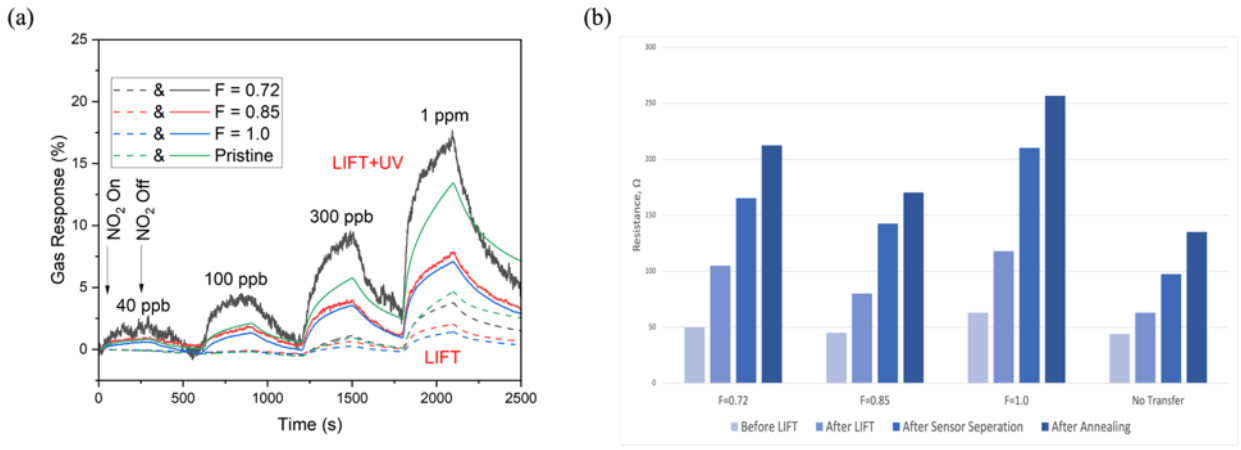

Fig. 4.14: (a) Temporal responses to NO_2 with (solid lines) and without (dashed lines) the UV illumination at various gas concentrations of the graphene + 5 nm ZrO_2 LIFTed graphene sensors via different fluences after the thermal annealing. (b) Resistance change in the graphene sensors before and after the LIFT, after the sensor separation and thermal annealing, in various fluences. "Pristine" refers to sensors without LIFT. The wavelength of UV light was 365 nm, and its intensity was ~10 mW/cm^2. Responses were recorded in dry air at room temperature (22 ℃).

In the absence of UV illumination, the NO_2 sensing performance of the graphene + 5 nm ZrO_2 LIFTed graphene sensors was observed to improve at all fluences, as evidenced by the data presented as dashed lines in *Fig.* 4.14 *(a)*. This improvement may be attributed to the creation of additional adsorption sites on the sensor surface due to thermal annealing. However, under UV illumination, the relative NO_2 sensing responses of the LIFTed sensors at various fluences exhibited a reduction post-annealing, with a decrease of approximately 17% observed for the F=0.72 J/cm^2 fluence at 1 ppm. Furthermore, thermal annealing increased the resistance of all sensors, as demonstrated in *Fig.* 4.14 *(b)*. After the thermal annealing, it was observed that despite the lower NO_2 sensing, the response was faster.

During the NO_2 sensing experiment, an unusual phenomenon was observed subsequent to the introduction of UV (365 nm) illumination, where the conductance of all sensors was decreased dramatically, as shown in *Fig.* 4.15. Notably, the conductance decrease was two orders of magnitude higher than in the previous NO_2 sensing measurements after the introduction of UV illumination. The conductance saturation levels of each graphene sensor vary significantly, depending on the fluence to which they were LIFTed. The pristine graphene sensor exhibited the highest saturated conductance, followed by sensors LIFTed with F=1.0, F=0.85, and F=0.72 J/cm^2

fluences, respectively. Although one can speculate that the observed conductance drop can be attributed to the altered graphene surface structure via thermal annealing, further investigation is still required.

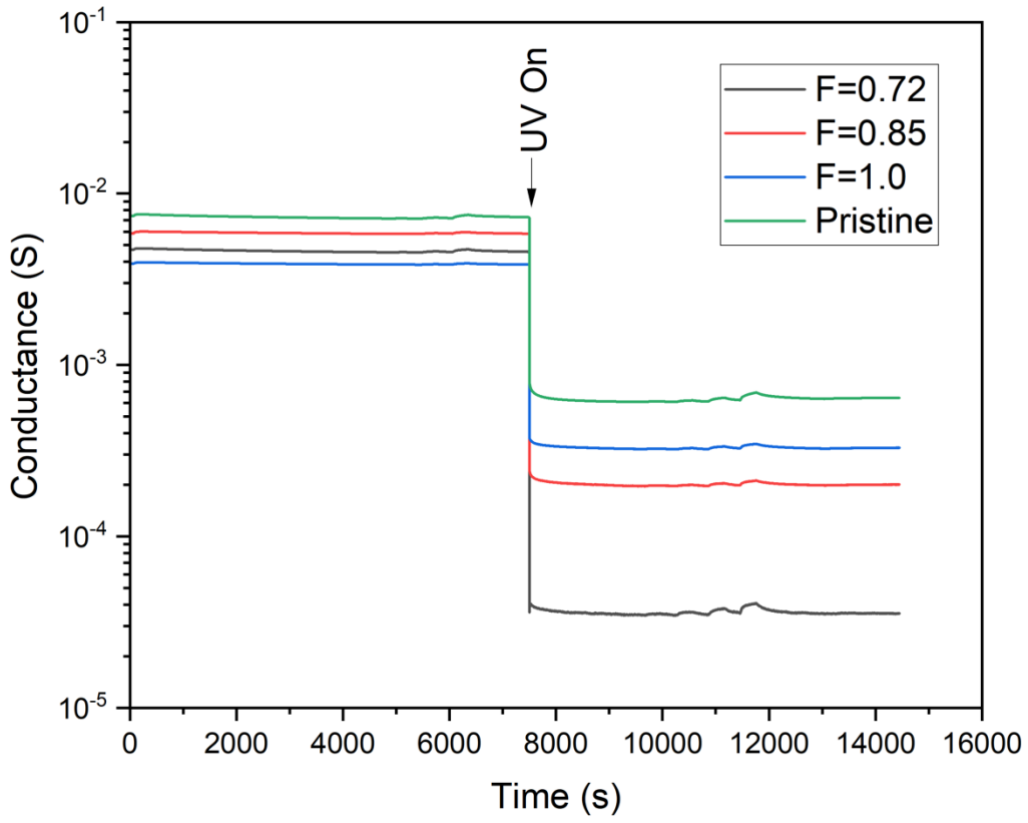

Fig. 4.15: Conductance change (Siemens) upon the UV illumination of the graphene sensors LIFTed with graphene + 5 nm ZrO_2 via various fluences. The wavelength of UV light was 365 nm, and its intensity was ~10 mW/cm^2. Responses were recorded in dry air at room temperature (22 °C). The conductance values are presented on a logarithmic scale.

5. Summary

LIFT is a printing technique where a material layer is transferred from the donor substrate to the receiver substrate by an action of a laser beam. This study aimed to investigate the role of graphene as a donor substrate, receiver substrate, and release layer in the blister-based LIFT. Furthermore, the study sought to evaluate the potential of the BB-LIFT technique for the functionalisation of graphene-based gas sensors with graphene and metal oxide (ZrO_2). To assess the gas sensing capabilities of the sensors, their responses to environmentally hazardous NO_2 gas were measured from 40 ppb to 1 ppm in the air.

First, the experiment geometry and a suitable range of laser pulse parameters were established at CVD graphene transfer from an Al-coated quartz substrate to a SiO_2-coated Si substrate. The transferred graphene retained its atomic structure and appeared on the receiver substrate as micron-sized islands (flakes), as confirmed by Raman spectroscopy measurements, SEM and optical microscopy images. At laser pulse energy densities of 0.7-1.0 J/cm^2 (laser wavelength 248 nm, pulse length 25 ns), the blister layer (Al) remained intact while the intended material was transferred.

Subsequent experiments focused on transferring thin (0.5-50 nm) ZrO_2 layers onto the graphene-coated sensor substrates via BB-LIFT. It was established that the oxide layer was successfully transferred only when a graphene layer was inserted between the Al and oxide layers. The SEM images of the receiver substrate showed no transfer in the case of solely ZrO_2-coated donor substrate. This result highlights the crucial role of graphene as a release layer for ZrO_2 transfer. Although some graphene was also transferred with ZrO_2, the critical role of graphene was enabling the transfer of ZrO_2. This outcome can be attributed to the strong bonding between the Al and ZrO_2 layers, which hinders the successful transfer of ZrO_2.

The NO_2 sensing measurements did not show an increase in the sensitivity of graphene sensors after ZrO_2 BB-LIFT compared to pristine ones. This was attributed to the weak coupling of the transferred material with underlying graphene so that the gas adsorption on oxides is not altering the electronic properties of graphene on receiving substrate. The ZrO_2 flakes merely hung on the surface without actively participating in sensor action through electronic interaction.

Thermal annealing at 500 °C for 3 hours in the vacuum chamber was performed on the graphene sensor to promote interaction between the graphene surface and the transferred ZrO_2. The NO_2 sensing measurement of this annealed sensor revealed an improvement in the response rate at

measured NO_2 concentrations. However, an increase in sensitivity compared to the pristine sensor was still not observed. When illuminated by UV light (365 nm), the conductance of the sensors dropped by approximately two orders of magnitude, which was an unusual response compared to the measurements reported in the literature. While the reason for this behaviour remains unknown, further investigation is required to understand this phenomenon.

The main novelty of this research lies in revealing the importance of graphene as a release layer for ultra-thin ZrO_2 transfer via the BB-LIFT technique. Future research can explore the chemical composition of the graphene sensor surface following BB-LIFT using energy-dispersive X-ray (EDX) analysis. Furthermore, an in-depth investigation into the release layer properties of graphene can be conducted by utilising novel materials in the BB-LIFT technique. Although the robustness of the BB-LIFT method utilised with a graphene release layer enables to transfer of ultra-thin metal oxides rapidly at room temperature without requiring any vacuum conditions or post-chemical treatment, improvement in gas sensing characteristics requires further research efforts to ultimately enable the efficient detection of environmentally hazardous NO_2 gas.

Acknowledgements

I would like to extend my deepest gratitude and appreciation to the individuals and organisations who have provided invaluable support throughout my master's thesis journey.

First and foremost, I am immensely grateful to my supervisors, Prof. Raivo Jaaniso and Dr Margus Kodu, for their guidance, expertise, and unwavering encouragement. Their educational approach, imparting technical knowledge of experimental setups, fostering familiarity with the laboratory environment, and providing insightful feedback, have played a pivotal role in shaping the direction and quality of this research.

I am indebted to Prof. Siim Pikker for sharing valuable knowledge on SEM and assisting me in obtaining high-quality images through his supportive approach. Additionally, I would like to express my gratitude to Prof. Valter Kiisk for his meticulous laser-cutting work and informative assistance throughout the process. I am also thankful to the contributors from the Institute of Physics at the University of Tartu for their assistance in sample preparations and insightful instructions.

I extend my sincere appreciation to the esteemed members of the Laboratory of Sensor Technology at the University of Tartu. Their friendly atmosphere, vast knowledge, intellectual contributions, and constructive criticism have greatly enriched my understanding and propelled the advancement of this work.

Lastly, I am profoundly grateful to my family for their unwavering encouragement, unconditional love, and steadfast belief in my abilities. Their continuous support throughout this challenging journey has been a constant source of motivation and inspiration.

References

[1] World Health Organization. (2021). WHO global air quality guidelines: particulate matter (PM2. 5 and PM10), ozone, nitrogen dioxide, sulfur dioxide, and carbon monoxide.

[2] Novoselov, K. S., Geim, A. K., Morozov, S. V., Jiang, D. E., Zhang, Y., Dubonos, S. V., ... & Firsov, A. A. (2004). Electric field effect in atomically thin carbon films. *science*, *306*(5696), 666-669.

[3] Schedin, F., Geim, A. K., Morozov, S. V., Hill, E. W., Blake, P., Katsnelson, M. I., & Novoselov, K. S. (2007). Detection of individual gas molecules adsorbed on graphene. *Nature materials*, *6*(9), 652-655.

[4] Chakraborthy, A., Nuthalapati, S., Nag, A., Afsarimanesh, N., Alahi, M. E. E., & Altinsoy, M. E. (2022). A Critical Review of the Use of Graphene-Based Gas Sensors. *Chemosensors*, *10*(9), 355.

[5] Xie, T., Wang, Q., Wallace, R. M., & Gong, C. (2021). Understanding and optimisation of graphene gas sensors. *Applied Physics Letters*, *119*(1), 013104.

[6] Sun, D., Luo, Y., Debliquy, M., & Zhang, C. (2018). Graphene-enhanced metal oxide gas sensors at room temperature: A review. *Beilstein journal of nanotechnology*, *9*(1), 2832-2844.

[7] Rivera, I. F., Joshi, R. K., & Wang, J. (2010, November). Graphene-based ultra-sensitive gas sensors. In *SENSORS, 2010 IEEE* (pp. 1534-1537). IEEE.

[8] He, Q., Wu, S., Yin, Z., & Zhang, H. (2012). Graphene-based electronic sensors. *Chemical Science*, *3*(6), 1764-1772.

[9] Ko, G., Kim, H. Y., Ahn, J., Park, Y. M., Lee, K. Y., & Kim, J. (2010). Graphene-based nitrogen dioxide gas sensors. *Current Applied Physics*, *10*(4), 1002-1004.

[10] Sawada, K., Tanaka, T., Yokoyama, T., Yamachi, R., Oka, Y., Chiba, Y., ... & Uchida, K. (2020). Co-porphyrin functionalized CVD graphene ammonia sensor with high selectivity to disturbing gases: hydrogen and humidity. *Japanese Journal of Applied Physics*, *59*(SG), SGGG09.

[11] Mortazavi Zanjani, S. M., Sadeghi, M. M., Holt, M., Chowdhury, S. F., Tao, L., & Akinwande, D. (2016). Enhanced sensitivity of graphene ammonia gas sensors using molecular doping. *Applied Physics Letters*, *108*(3), 033106.

[12] Lv, R., Chen, G., Li, Q., McCreary, A., Botello-Méndez, A., Morozov, S. V., ... & Terrones, M. (2015). Ultrasensitive gas detection of large-area boron-doped graphene. *Proceedings of the National Academy of Sciences*, *112*(47), 14527-14532.

[13] Ma, J., Zhang, M., Dong, L., Sun, Y., Su, Y., Xue, Z., & Di, Z. (2019). Gas sensor based on defective graphene/pristine graphene hybrid towards high sensitivity detection of NO2. *AIP Advances*, *9*(7), 075207.

[14] Cho, B., Yoon, J., Hahm, M. G., Kim, D. H., Kim, A. R., Kahng, Y. H., ... & Ko, H. C. (2014). Graphene-based gas sensor: metal decoration effect and application to a flexible device. *Journal of Materials Chemistry C*, *2*(27), 5280-5285.

[15] Ni, Z. H., Wang, H. M., Luo, Z. Q., Wang, Y. Y., Yu, T., Wu, Y. H., & Shen, Z. X. (2010). The effect of vacuum annealing on graphene. *Journal of Raman Spectroscopy: An International*

Journal for Original Work in all Aspects of Raman Spectroscopy, Including Higher Order Processes, and also Brillouin and Rayleigh Scattering, *41*(5), 479-483.
[16] Yang, C. M., Chen, T. C., Yang, Y. C., & Meyyappan, M. (2019). Annealing effect on UV-illuminated recovery in gas response of graphene-based NO 2 sensors. *RSC advances*, *9*(40), 23343-23351.
[17] Kumar, R., Liu, X., Zhang, J., & Kumar, M. (2020). Room-temperature gas sensors under photoactivation: from metal oxides to 2D materials. *Nano-Micro Letters*, *12*, 1-37.
[18] Kodu, M., Berholts, A., Kahro, T., Eriksson, J., Yakimova, R., Avarmaa, T., ... & Jaaniso, R. (2019). Graphene-based ammonia sensors functionalised with sub-monolayer V2O5: A comparative study of chemical vapour deposited and epitaxial graphene. *Sensors*, *19*(4), 951.
[19] Lin, J., Zhong, J., Kyle, J. R., Penchev, M., Ozkan, M., & Ozkan, C. S. (2011). Molecular absorption and photodesorption in pristine and functionalized large-area graphene layers. *Nanotechnology*, *22*(35), 355701.
[20] Berholts, A., Kahro, T., Floren, A., Alles, H., & Jaaniso, R. (2014). Photo-activated oxygen sensitivity of graphene at room temperature. *Applied Physics Letters*, *105*(16), 163111.
[21] Wang, C., Yin, L., Zhang, L., Xiang, D., & Gao, R. (2010). Metal oxide gas sensors: sensitivity and influencing factors. *sensors*, *10*(3), 2088-2106.
[22] Arafat, M. M., Dinan, B., Akbar, S. A., & Haseeb, A. S. M. A. (2012). Gas sensors based on one dimensional nanostructured metal-oxides: a review. *Sensors*, *12*(6), 7207-7258.
[23] Dey, A. (2018). Semiconductor metal oxide gas sensors: A review. *Materials science and Engineering: B*, *229*, 206-217.
[24] Sun, D., Luo, Y., Debliquy, M., & Zhang, C. (2018). Graphene-enhanced metal oxide gas sensors at room temperature: A review. *Beilstein journal of nanotechnology*, *9*(1), 2832-2844.
[25] Wang, C., Wang, Y., Yang, Z., & Hu, N. (2021). Review of recent progress on graphene-based composite gas sensors. *Ceramics International*, *47*(12), 16367-16384.
[26] Kodu, M., Berholts, A., Kahro, T., Avarmaa, T., Kasikov, A., Niilisk, A., ... & Jaaniso, R. (2016). Highly sensitive NO2 sensors by pulsed laser deposition on graphene. *Applied Physics Letters*, *109*(11), 113108.
[27] Kodu, M., Berholts, A., Kahro, T., Kook, M., Ritslaid, P., Seemen, H., ... & Jaaniso, R. (2017). Graphene functionalised by laser-ablated V2O5 for a highly sensitive NH3 sensor. *Beilstein journal of nanotechnology*, *8*(1), 571-578.
[28] Tang, X., Debliquy, M., Lahem, D., Yan, Y., & Raskin, J. P. (2021). A review on functionalized graphene sensors for detection of ammonia. *Sensors*, *21*(4), 1443.
[29] Morales, M., Munoz-Martin, D., Marquez, A., Lauzurica, S., & Molpeceres, C. (2018). Laser-induced forward transfer techniques and applications. *Advances in Laser Materials Processing*, 339-379.
[30] Serra, P., & Piqué, A. (2019). Laser-induced forward transfer: fundamentals and applications. *Advanced Materials Technologies*, *4*(1), 1800099.
[31] Piqué, A., & Serra, P. (Eds.). (2018). Laser printing of functional materials: 3D microfabrication, electronics and biomedicine. John Wiley & Sons.

[32] Smits, E. C., Walter, A., De Leeuw, D. M., & Asadi, K. (2017). Laser induced forward transfer of graphene. *Applied Physics Letters*, *111*(17), 173101.
[33] Childres, I., Jauregui, L. A., Park, W., Cao, H., & Chen, Y. P. (2013). Raman spectroscopy of graphene and related materials. *New developments in photon and materials research*, *1*, 1-20.
[34] Palla-Papavlu, A., Dinescu, M., Wokaun, A., & Lippert, T. (2014). Laser-induced forward transfer of single-walled carbon nanotubes. *Applied Physics A*, *117*, 371-376.
[35] Wang, X., Zhang, J., Mei, X., Miao, J., & Wang, X. (2021). Laser-induced forward transfer of graphene oxide. *Applied Physics A*, *127*, 1-9.
[36] Schultze, V., & Wagner, M. (1991). Laser-induced forward transfer of aluminium. *Applied surface science*, *52*(4), 303-309.
[37] Papadopoulou, E. L., Axente, E., Magoulakis, E., Fotakis, C., & Loukakos, P. A. (2010). Laser induced forward transfer of metal oxides using femtosecond double pulses. *Applied surface science*, *257*(2), 508-511.
[38] Zhao, J., & Hu, Y. (2019). Surface morphology formation of Ti films in laser-induced forward transfer. *Surface Topography: Metrology and Properties*, *7*(2), 025022.
[39] Goodfriend, N. T. (2018). *Advancements and understanding of Blister-Based Laser-Induced Forward-Transfer* (Doctoral dissertation, University of Edinburgh).
[40] Kononenko, T. V., Nagovitsyn, I. A., Chudinova, G. K., & Mihailescu, I. N. (2010). Application of clean laser transfer for porphyrin micropatterning. *Applied surface science*, *256*(9), 2803-2808.
[41] Komlenok, M. S., Kudryavtsev, O. S., Pasternak, D. G., Vlasov, I. I., & Konov, V. I. (2021). Blister-Based Laser-Induced Forward Transfer of Luminescent Diamond Nanoparticles. *physica status solidi (a)*, *218*(5), 2000269.
[42] Kononenko, T. V., Alloncle, P., Konov, V. I., & Sentis, M. (2009). Laser transfer of diamond nanopowder induced by metal film blistering. *Applied Physics A*, *94*, 531-536.
[43] Arutyunyan, N. R., Komlenok, M. S., Kononenko, T. V., Dezhkina, M. A., Popovich, A. F., & Konov, V. I. (2019). Printing of single-wall carbon nanotubes via blister-based laser-induced forward transfer. *Laser Physics*, *29*(2), 026001.
[44] Komlenok, M. S., Pivovarov, P. A., Dezhkina, M. A., Rybin, M. G., Savin, S. S., Obraztsova, E. D., & Konov, V. I. (2020). Printing of crumpled CVD graphene via blister-based laser-induced forward transfer. *Nanomaterials*, *10*(6), 1103.
[45] Zande, A. M. V. D., Barton, R. A., Alden, J. S., Ruiz-Vargas, C. S., Whitney, W. S., Pham, P. H., ... & McEuen, P. L. (2010). Large-scale arrays of single-layer graphene resonators. *Nano letters*, *10*(12), 4869-4873.

Appendix A

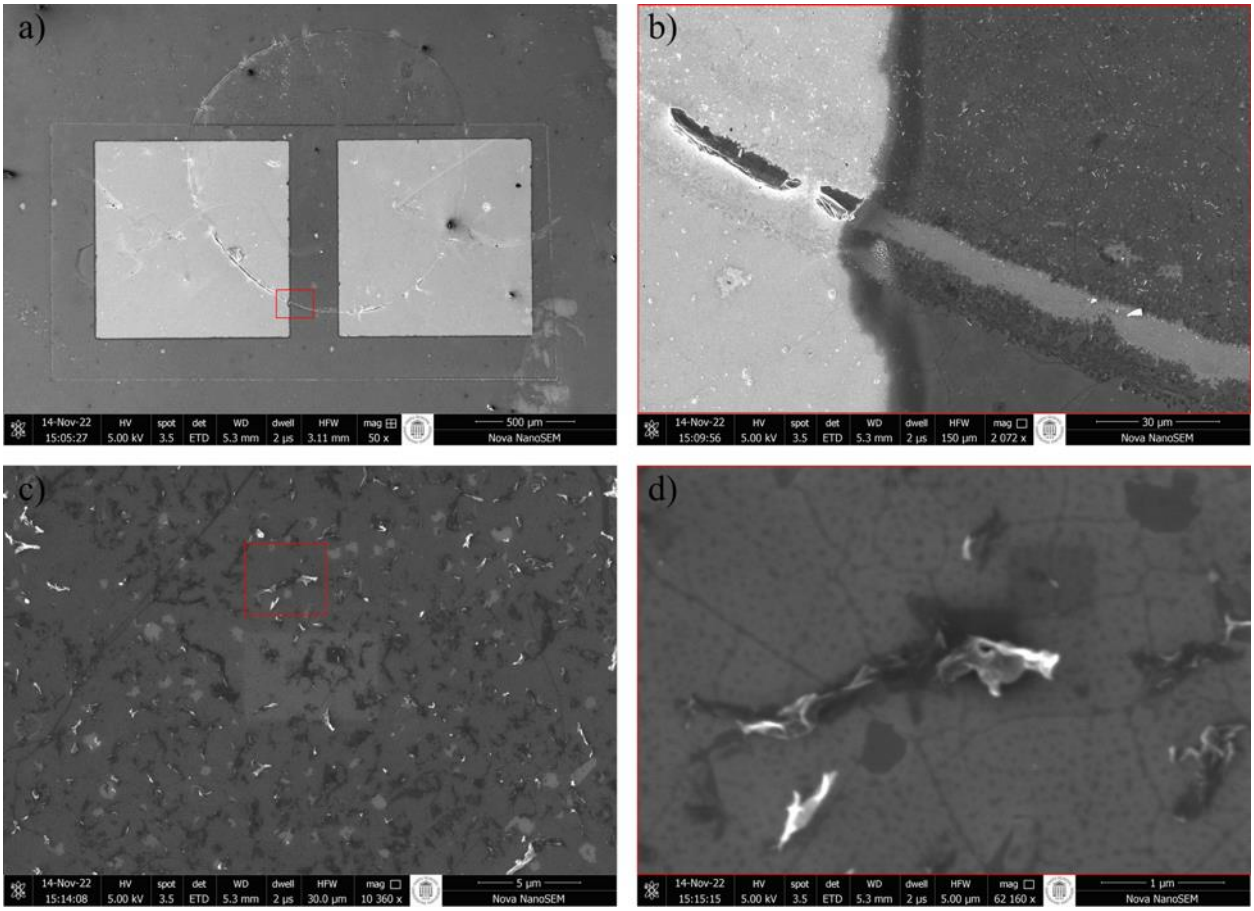

Fig. B: SEM images of the pristine graphene LIFTed graphene gas sensor via F=1.0 J/cm^2 fluence. (a) The LIFTed area between the electrodes. (b) Magnified view of the red rectangle from (a), exhibiting an edge of the LIFTed area. (c) Graphene flakes in the LIFTed area. (d) The magnified image of the red rectangle from (c) illustrates a graphene flake.

Appendix B

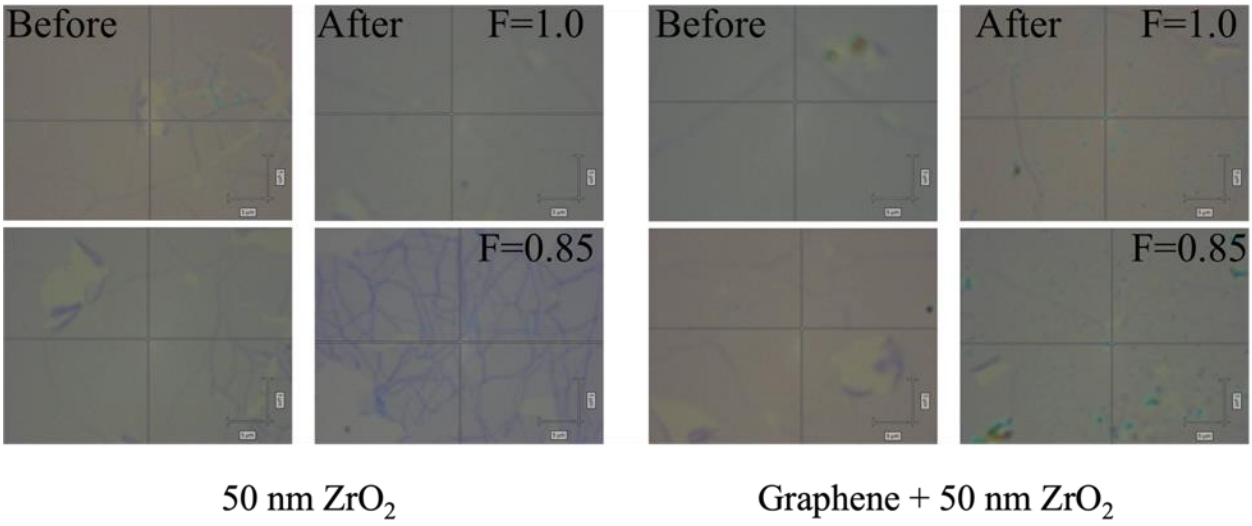

Fig. A: Optical microscope images between the electrodes of the graphene gas sensors before and after the LIFT with 50 nm ZrO_2 on the left and graphene + 50 nm ZrO_2 on the right. The optical microscope image scale is 5 μm.

Licence

To the vice dean for academic affairs of the Faculty of Science and Technology, University of Tartu

Application for establishing restrictions on the publishing of the graduation thesis, and declaring the defence private

Name	Ahmet Burak Baloglu
Date of birth	28.09.1994
Curriculum	Materials Science and Technology
Supervisor	Dr. Margus Kodu and Dr. Raivo Jaaniso
Graduation thesis title	Graphene in blister-based LIFT

[X] I request my graduation thesis not to be published until 29.05.2026 (date) for the reason indicated below:

- [ ] Economic copyright rights belong to other people
- [ ] Thesis includes personal data and the data subject has not agreed to publishing
- [ ] State secret
- [ ] Trade secret
- [X] In future, the graduation thesis will be published as a scientific article
- [ ] Other reasons

Explanation (reasons why restrictions are applied for and why for the particular period):

The thesis includes results that will be published in scientific journal. However, it might be necessary to obtain some additional results before publishing. This will take some time.

☐ I request my defence to be declared private.

Explanation (reasons for declaring the defence private):

Application has the following annexes (to be filled in if there are annexes, i.e. the company's confirmation that the thesis involves a trade secret):

1.

2.

Date and student's signature	Signed digitally
Date and supervisor's signature	Signed digitally